

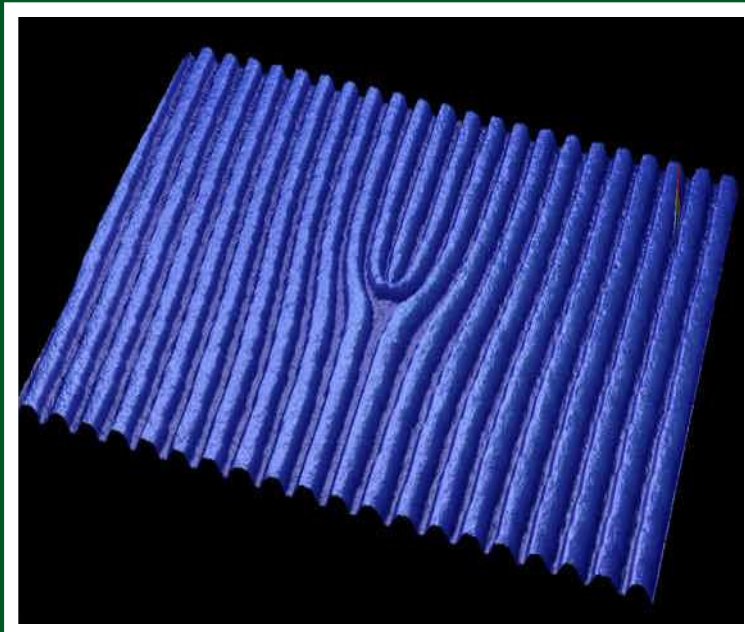
AJP

ISSN: 0971-3093

Vol 25, No 7, July, 2016

ASIAN JOURNAL OF PHYSICS

An International Research Journal



ap

ANITA PUBLICATIONS

FF-43, 1st Floor, Mangal Bazar, Laxmi Nagar, Delhi-110 092, India

B O : 2, Pasha Court, Williamsville, New York-14221-1776, USA



Silicon Photonics Technology: Ten Years of Research at IIT Madras

B K Das, N Das Gupta, S Chandran, S Kurudi, P Sah, R Nandi, Ramesh K, Sumi R, S Pal,
S Kaushal, S M Sundaram, P Sakthivel, Sidharth R, R Joshi, H Sasikumar, U Karthik,
S Krubhakar, G R Bhatt, J P George, R K Navalakhe, Narendran R, and I Seethalakshmi

Integrated Optoelectronics Labs, Department of Electrical Engineering, IIT Madras, Chennai - 600 036, India

The integrated optoelectronics research group at IIT Madras has been active since 2007 with a determination towards developing a center of excellence for silicon photonics research. The core research theme involves novel designs, CMOS compatible fabrication process optimizations and subsequent experimental demonstrations leading towards cost-effective, energy-efficient and high-speed optoelectronic interconnects for various applications. As of now, various prototype devices like power splitters, ITU channel interleavers, variable optical attenuators, p-i-n phase shifters/modulators, ring resonators, DBR filters etc., have been demonstrated by exploiting conventional microelectronics technology as well as recently established nano-fabrication facilities at IIT Madras. Their design principle, process development, fabrication and characterizations are described in the present article. © Anita Publications. All rights reserved.

Keywords: Optoelectronics, Silicon photonics, p-i-n phase shifters/modulators, Ring resonators, DBR filters

1 Introduction

The need of optical interconnections was emphasized comprehensively for the first time by Goodman *et al* in 1984 [1]. The progress in this subject was reviewed and re-emphasized again in 2000 by another landmark article by David A B Miller [2]. Further, in 2010, Young and his colleagues presented an overview on how optical input/output technology was being implemented for highly demanding tera-scale computing systems [3]. Finally, silicon optical interconnect or silicon photonics is finding its realistic applications in mainstream semiconductor industry, mainly because of its potentiality in high-speed and energy-efficient data transfer through second and third generation optical communication wavelengths ($1.3 \mu\text{m} \leq \lambda \leq 1.6 \mu\text{m}$) [4-6].

Besides passive on-chip optical networking devices, optoelectronic devices like lasers, photodetectors, variable optical attenuators, modulators/switches, tunable filters, etc. are essential for optical interconnect solutions. Being an indirect bandgap semiconductor ($E_g = 1.12 \text{ eV}$), silicon does not qualify for an efficient light emission. Therefore, hybrid integration of direct bandgap III-V semiconductors is being implemented [7]. As the conventional Si photodetectors are not suitable for communication wavelengths, Ge/SiGe photodetectors are being monolithically integrated in silicon-on-insulator (SOI) [8]. The plasma dispersion effect is efficiently used for high-speed modulator and switching devices in SOI platform using *state-of-the-art* CMOS technology [9]. Here, modulation or switching is based on localized refractive index modulation by switching free carrier distribution. The carrier concentrations can be controlled by suitable biasing and modulation voltage of p-i-n/p-n junction fabricated across a waveguide. The flip-side of the plasma dispersion effect is the change in imaginary part of the dielectric constant, which eventually causes optical absorption/attenuation. Nevertheless, this is being exploited to design electronically controlled variable optical attenuators

Corresponding author

e-mail: bkdas@ee.iitm.ac.in (B K Das)

[10]. However, in reconfigurable devices, where switching speed is not an issue, the excellent thermo-optic effect in silicon crystal is utilized for cost-effective solutions [11-14]. All-optical signal processing is another important area of research, as tightly confined guided modes in a silicon waveguide enable strong nonlinear interactions [15].

Though the interests in silicon photonics research among Indian scientists and engineers were noticeable here and there, no planned long-term research goals were set until a decade ago. IIT Madras (India) took the lead to start a silicon photonics research group in 2006. Since then the group at IIT Madras has been actively engaged in novel design, fabrication and characterizations of silicon photonics devices for communication systems and sensor applications. By the end of 2011, various prototype devices were demonstrated by making use of conventional i-line lithography technology (1- μm node) available at IIT Madras [16-19]. With the availability of nanofabrication facilities at the Centre for NEMS and Nanophotonics (funded by MeitY Govt. of India), the research program was raised to the next level during last couple of years – research outcomes have been presented in international conferences, published in peer reviewed journals, and as filed patents [20-33]. The goal of the research group is now set to carry out world class silicon photonics research encompassing novel device designs, CMOS compatible fabrication process optimizations and experimental demonstrations leading towards cost-effective, energy-efficient and high-speed optoelectronic interconnects for various applications. In this article, we would like to highlight the unique development of silicon photonics technology that has been taking place during last ten years at IIT Madras. We believe this review article will help students, research scholars and perhaps many other research groups in India and abroad who are aspiring to step into this important area of research.

In section 2, we will discuss details of commercially available SOI substrates and their suitability as a silicon photonics platform. The basic building blocks like single-mode/multi-mode waveguide design rule, principle of multimode interference and directional coupler will be also discussed in this section. In section 3, a generic fabrication flow for the waveguide, micro-heaters, p-type/n-type diffusion doping for active control of a guided mode will be discussed. Various devices fabricated with 5- μm , 2- μm , and 250-nm SOI substrates will be discussed in sections-4, 5, and 6, respectively. Finally the conclusion is given in section 7.

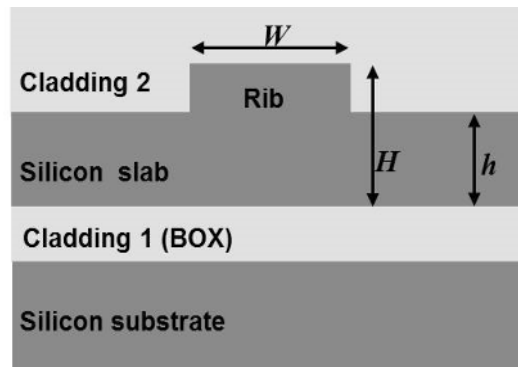
2 Optical waveguides in SOI platform - Design Rules

The success of silicon photonics came with the commercial availability of optical-grade SOI wafers in the first decade of this millennium. Prior to this, electronic-grade doped SOI wafers (p-type or n-type device layer) were mainly used in large-scale integration of nano-scale electronic devices in a drive to sustain Moore's law [34]. As the advanced CMOS technology paved the way for ultra-large-scale integrated electronic circuits, the necessity of on-chip high-speed optical interconnects has been increasing. Low-loss optical waveguide in SOI platform with Si as core material is the key to on-chip high-speed optical interconnects. In fact, SOI substrate itself could provide 1D waveguide with buried oxide (BOX) as bottom cladding, intrinsic silicon device layer as core and air/silicon dioxide as top cladding. The 2D waveguide can be designed with rib and/or with rectangular silicon core and air/SiO₂ cladding. In this section, we discuss the design aspects of three basic waveguide systems, namely, single-mode, multimode and coupled waveguides.

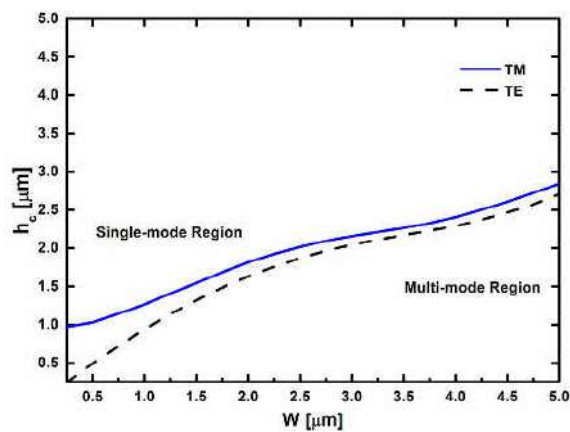
2.1 Single-mode waveguides

Besides propagation loss, an optical waveguide must be defined by other figure of merits like birefringence (polarization dependency) and dispersion effects (wavelength dependency), modal confinement factor, sharp bends (minimum waveguide bending radius) and capability of handling impedance/mode-size mismatch with input/output fibers. However, controlling all these properties simultaneously is a challenging task. In order to achieve compact integrated optical devices with smaller bend radius; core-cladding index

difference should be high enough such that the guided mode is tightly confined within the core. Again as the index contrast is high, the waveguide cross-section has to be small enough to make the waveguide single mode (supporting only the fundamental mode). Further, the smaller cross-section makes the waveguide highly wavelength dependent (dispersive) as well as lossy. The loss is mainly due to the enhanced interaction of guided modes with sidewall surface roughness, dimensional non-uniformities, etc. An optical waveguide supporting only the fundamental mode is essentially used in optical interconnect applications to reduce the circuit complexity. Typical cross-sectional view of a SOI waveguide is shown in Fig 1(a); single-mode guidance for a given operating wavelength band ($\lambda \sim 1550$ nm) is achieved by selecting appropriate values of three parameters namely, waveguide width W , height H , slab thickness h (see Fig 1(a)). Depending on applications, one can achieve desired modal confinements, dispersion characteristics, and polarization dependencies, etc. by suitably scaling these three parameters. Relatively, larger cross-section rib waveguides (5- μm SOI) with $W \sim 5$ μm , $H \sim 5$ μm and $h \sim 4$ μm are used for wavelength independent, dispersion free and polarization independent photonic circuits [20, 35]. In addition, efficient chip-to-fiber light coupling is possible with larger waveguide structures [36]. Devices with waveguide width ~ 2 μm (2- μm SOI) have been proposed for large-scale manufacturing of photonics transceiver solutions [37]. Commercially available lensed fiber tip with a focused spot-size diameter of ~ 2 μm can be used efficiently for coupling light into 2- μm SOI waveguide. Submicron single-mode waveguide geometry (fabricated with 250 nm SOI), with typical design parameters of $W \sim 500$ nm, $H \sim 250$ nm and $h < 200$ nm (photonic wire waveguide) are used to design compact structures such as microring resonators of radius as small as 3 μm [38].



(a)



(b)

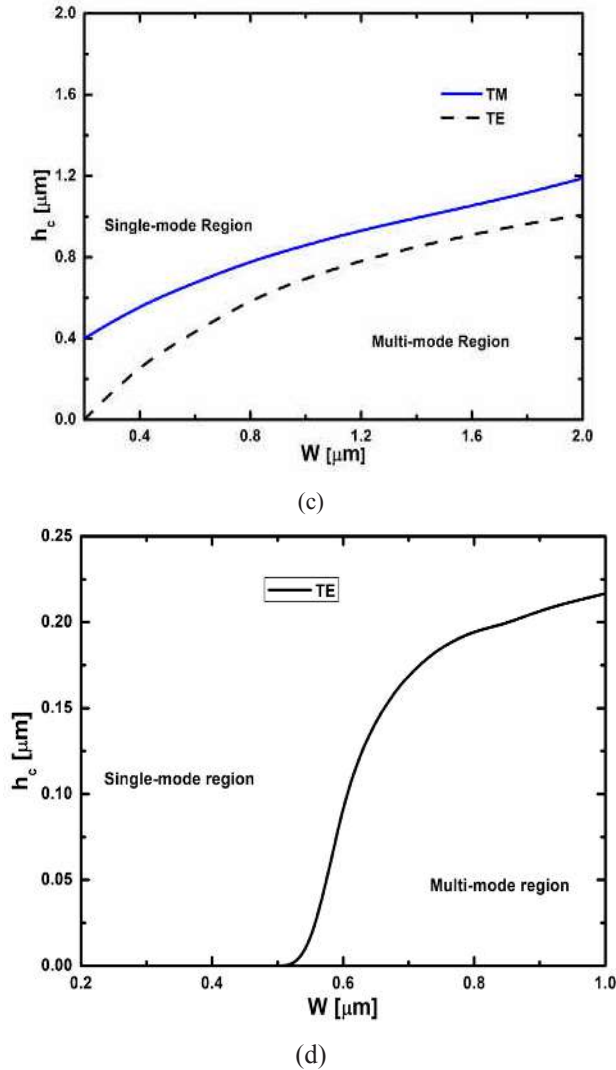
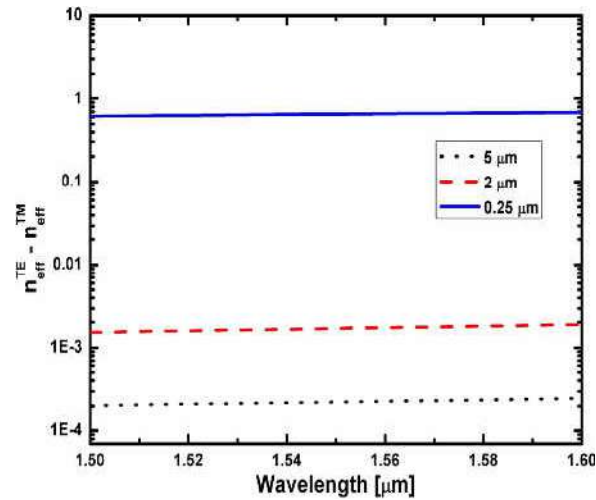


Fig 1. (a) Schematic cross-sectional view of a SOI optical waveguide; W - width, H - height (device layer thickness), h - thickness of slab, BOX - buried oxide (SiO_2); (b), (c) and (d) are the calculated slab height cut-off h_c for single-mode guidance ($\lambda \sim 1550$ nm) as a function of waveguide width W for device layer thickness of $5 \mu\text{m}$, $2 \mu\text{m}$, and 250 nm, respectively. Since submicron rectangular photonic wire waveguides are highly polarization sensitive with width variation, h_c is shown only for TE-like mode.

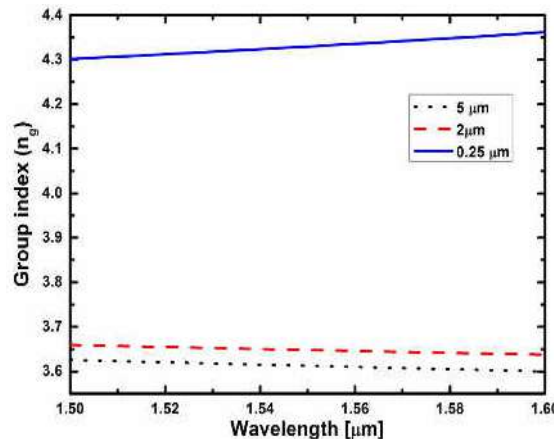
A generic rib waveguide geometry (as shown in Fig 1(a)) is used to evaluate slab height cut-off h_c as a function of W , for single-mode guidance at an operating wavelength $\lambda \sim 1550$ nm for device layer thickness $H = 5 \mu\text{m}$, $2 \mu\text{m}$ and 250 nm, respectively. Lumerical MODE solver is used for simulations and the extracted results have been shown in Figs 1 (b)-(d). The simulation results were obtained for both TE-like and TM-like modes. However, we have shown results only for TE-like hybrid mode in case of 250 nm device layer thickness as TM-like hybrid modes are found leaky for certain slab thicknesses.

Theoretical calculations also reveal that the single-mode waveguides with larger device layer thickness offer nearly a polarization independent properties (in terms of mode-size and effective index of the

guided mode). Figure 2(a) shows the wavelength dependent structural birefringence comparison of typical single-mode waveguides with device layer thickness of 5 μm , 2 μm and 250 nm, respectively: black dotted line represents the birefringence of a waveguide with $W = 5 \mu\text{m}$, $H = 5 \mu\text{m}$ and $h = 4 \mu\text{m}$; dashed red line represents the birefringence of a waveguide with $W = 1.5 \mu\text{m}$, $H = 2 \mu\text{m}$ and $h = 1 \mu\text{m}$; and solid blue line represents the birefringence of a waveguide with $W = 500 \text{ nm}$, $H = 250 \text{ nm}$ and $h = 0$. It is evident that the birefringence of larger cross-section waveguides is estimated to be very small ($< 10^{-3}$). However, the submicron photonic wire waveguide is found to be highly birefringent (> 0.7). Figure 2 (b) shows the comparison of group indices for 5 μm , 2 μm and 250 nm waveguides. As expected, waveguides with larger cross-sections are found to be nearly dispersion free over a wide range operating wavelengths; the photonic wire waveguides are found to be highly dispersive. This shows that integrated optical components/devices designed with submicron waveguides are wavelength sensitive.



(a)



(b)

Fig 2. (a) Birefringence and (b) group index comparison of various waveguide structures in SOI substrate. dotted (black), dashed (red), and solid (blue) lines represent birefringence of 5 μm waveguide ($W = 5 \mu\text{m}$, $H = 5 \mu\text{m}$ and $h = 4 \mu\text{m}$), 2 μm waveguide ($W = 1.5 \mu\text{m}$, $H = 2 \mu\text{m}$ and $h = 1 \mu\text{m}$) and 250 nm waveguide ($W = 500 \text{ nm}$, $H = 250 \text{ nm}$ and $h = 0$), respectively.

2.2 Multimode Waveguides

Though the single-mode waveguides are mostly preferred in designing integrated optical devices, multimode waveguides play vital role in some key functions e.g., adiabatically excited fundamental mode guidance in multimode waveguides offer low propagation loss, power splitter by appropriate interference of guided modes, low-loss switch matrix in on-chip optical networking, etc. Multimode interference coupler (MMIC) is found to be very attractive and frequently used to demonstrate many stand-alone integrated optical devices such as ring resonators [39], Mach-Zehnder interferometers [40], and arrayed waveguide gratings [41] due to nearly wavelength independent and polarization insensitive operation. MMIC structures are also found to be highly fabrication tolerant. An MMIC is comprised of input single-mode waveguide(s), a multi-mode waveguide section and output single-mode waveguide(s). Multi-mode section is designed to support higher order modes such that the interference of all the excited modes give rise to localized intensity distribution exactly similar to input intensity distribution and which can be explained well with self-imaging principle [42].

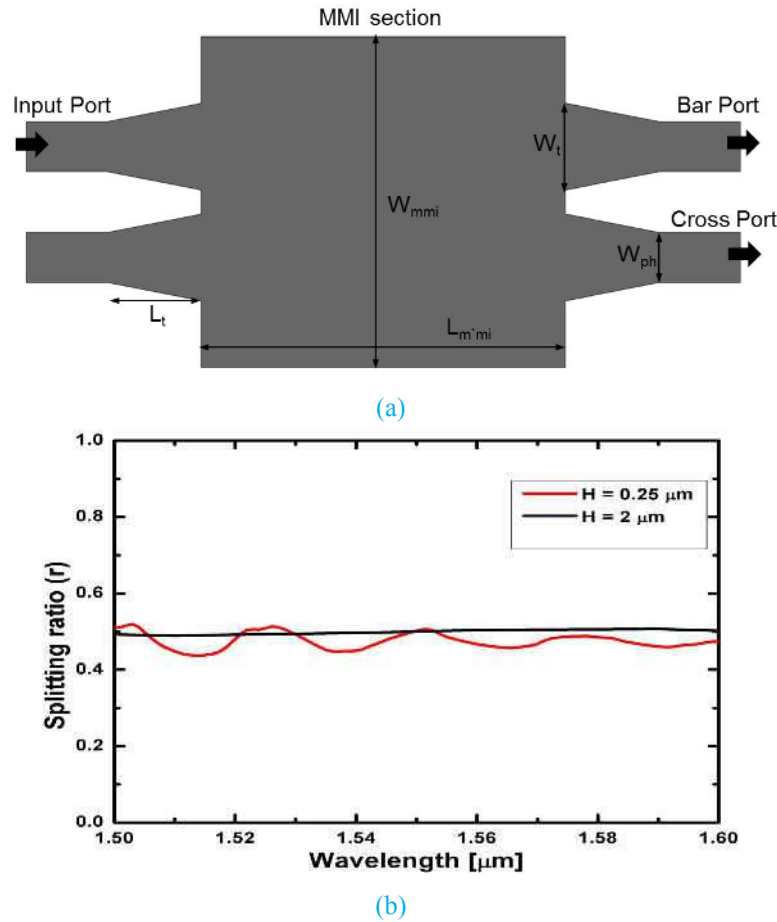


Fig 3. (a) Schematic top view of a 2×2 MMI coupler with input/output single-mode waveguides, where L_{mmi} – length of MMI section, W_{mmi} – width of MMI, W_t – taper width, W_{ph} – width of submicron waveguide and L_t – taper length. (b) Wavelength dependent 3-dB power splitting characteristics of a 2×2 MMICs designed with 2- μm SOI (red line) and 0.25 μm SOI. Calculations were carried out for TE-like guided modes.

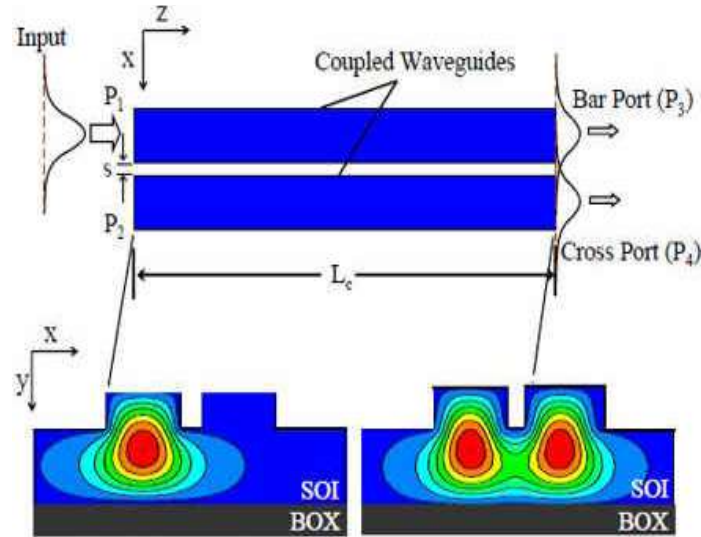
The localized spots formed in the multimode waveguide region can be tapped through the output waveguide(s) and thus the MMIC can be efficiently used as power splitter. In general, a multi-mode waveguide is defined by just increasing the width alone and maintaining the height of input, output and multi-mode waveguides. Higher the width of the multi-mode waveguide, more the number of modes supported by the waveguide and better the resolution of self-images. However, as width of MMIC section increases, the length at which self-images are formed also drastically increases. The length of MMIC can be greatly reduced without compromising the image resolution by properly positioning input waveguide(s) and exciting only certain guided modes in the multi-mode waveguide section. By utilizing paired interference property of MMIC, one can reduce the length of $2 \times N$ coupler for N fold images from $3L_\pi/N$ to L_π/N , where L_π is the beat length of the first two lowest order modes. We have used this property to design a 2×2 MMIC power splitter (see Fig 3(a)). According to paired interference condition for a $2 \times N$ MMIC, the input and output waveguide has to be positioned at $W_{\text{mmi}}^{\text{eff}}/6$, where $W_{\text{mmi}}^{\text{eff}}$ is the effective waveguide width of multimode waveguide section which is always higher than the actual width of the waveguide because of the existence of evanescent fields in either sides. However, because of large core-cladding refractive index contrast in SOI waveguides, the evanescent field strengths of guided modes are very small and hence $W_{\text{mmi}}^{\text{eff}}$ can be approximated to the physical width of the multi-mode waveguide section (W_{mmi}). Figure 3(a) shows the schematic view of typical 2×2 MMIC with input and output ends are interfaced with adiabatically tapered single-mode waveguides. The taper sections are attached to increase the coupling/collection efficiency and to reduce the impedance mismatch. The optimum waveguide parameters of the MMIC (for TE polarization) designed on $2 \mu\text{m}$ and $0.25 \mu\text{m}$ SOI substrates are summarized in Table 1. Figure 3(b) shows the wavelength dependent splitting ratio [$r = P_{\text{Cross}}/(P_{\text{Bar}} + P_{\text{Cross}})$] for $2 \mu\text{m}$ (black line) and $0.25 \mu\text{m}$ (red line) waveguides. The MMIC design using 2 micron device layer SOI is found to be nearly wavelength independent. Whereas the MMIC with submicron SOI device layer shows a slight wavelength dependent power splitting characteristics. Polarization dependency of the MMIC is also calculated and it is found that the variation of MMIC length (ΔL) is 0.6 % of L_{mmi} for $2 \mu\text{m}$ waveguide and 13 % for the $0.25 \mu\text{m}$ waveguide.

Table 1. Optimized MMIC parameters (for TE polarization) of micron sized waveguide cross-section ($H = 2 \mu\text{m}$) and submicron sized waveguide cross-section ($H = 0.25 \mu\text{m}$).

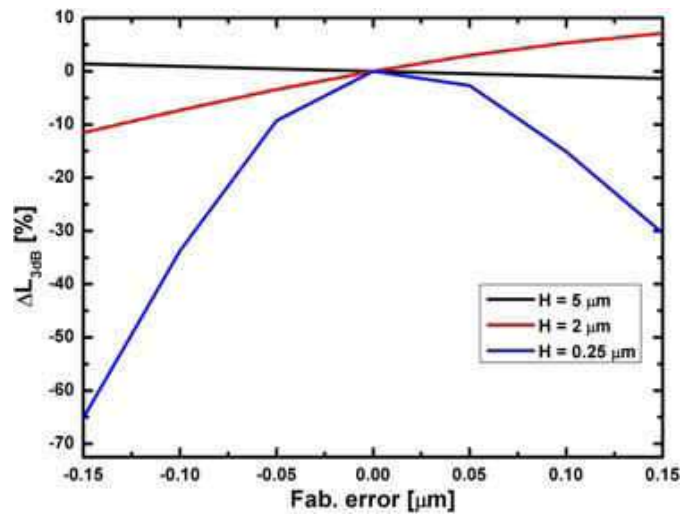
$H(\mu\text{m})$	$h(\mu\text{m})$	$W_{\text{ph}}(\mu\text{m})$	$W_{\text{t}}(\mu\text{m})$	$L_{\text{t}}(\mu\text{m})$	$W_{\text{mmi}}(\mu\text{m})$	$L_{\text{mmi}}(\mu\text{m})$
2	1	1.5	3	27	15	350
0.25	0	0.5	1	5	3.6	15

2.3 Coupled waveguides - Directional coupler

Waveguides are said to be coupled when they are exchanging power either in the co-direction or in the contra-direction propagations. Two parallel waveguides coupled co-directionally via evanescent fields of their guided modes are generally referred as a directional coupler (DC). The schematic top view of a typical DC is shown in Fig 4(a) and guided mode profiles at input and output of a 3-dB coupler are shown in the inset. When the waveguide separation is small enough such that the evanescent tails of the guided modes of the waveguides overlap each other causing the exchange of power between waveguides. The efficiency of coupling depends on the strength of evanescent field interaction between the coupled waveguides. DCs are mainly used as power splitters in integrated optical devices such as Mach-Zehnder interferometer, ring resonator, etc. The waveguide cross-section design parameters play a major role in obtaining desired performance of a DC. Figure 4(b) shows the 3-dB length variation from the design value of a DC as a function of fabrication error for $5 \mu\text{m}$, $2 \mu\text{m}$ and $0.25 \mu\text{m}$ waveguides. Considering lithographic limitations in respective technology nodes, the waveguide separations are chosen to be $2 \mu\text{m}$, $1 \mu\text{m}$ and $0.2 \mu\text{m}$, respectively.



(a)



(b)

Fig 4. Schematic top view of coupled waveguides in a directional coupler (3-dB) power splitter. L_c - 3 dB coupling length and s - waveguide separation. Guided mode profiles at the input and output regions are shown in the inset, (b) variation of 3-dB length of directional coupler as a function of fabrication error from designed values of 5 μm waveguide ($W = 5 \mu\text{m}$, $H = 5 \mu\text{m}$ and $h = 4 \mu\text{m}$), 2 μm waveguide ($W = 1.5 \mu\text{m}$, $H = 2 \mu\text{m}$ and $h = 1 \mu\text{m}$) and 0.25 μm waveguide ($W = 0.5 \mu\text{m}$, $H = 0.25 \mu\text{m}$ and $h = 0 \mu\text{m}$).

Conventionally, waveguide width is defined using either by photolithography or e-beam lithography, and ridge height is defined with subsequent reactive ion etching process. The etching can be precisely controlled. However, the width is highly dependent on the lithography process. If W is reduced/increased by ΔW because of fabrication error, the separation between the waveguides in a DC is increased/

reduced by same amount ΔW . Figure 4(b) shows the variation 3-dB length variation of the DC as function of fabrication error (ΔW). The designed cross-sections for 5 μm , 2 μm and 0.25 μm waveguides are same as the values used for birefringence calculation. The variation in 3dB length is defined as:

$$\Delta L_{3\text{dB}} [\%] = \frac{L_{3\text{dB}}^{\text{cal}} - L_{3\text{dB}}^{\text{Del}}}{L_{3\text{dB}}^{\text{Del}}} \times 100$$

where $L_{3\text{dB}}^{\text{cal}}$ is the calculated 3dB length with the respective fabrication error and $L_{3\text{dB}}^{\text{Del}}$ is the 3 dB length for a designed DC. The maximum 3-dB length variation for 5 μm waveguide is found to be 1.5%, whereas that for 2 μm and 250 nm waveguide DCs are 11% and 65%, for the fabrication error of 0.15 μm . This calculation shows that 250 nm waveguides are highly sensitive to fabrication errors compared to larger waveguide dimensions such as 2 μm or 5 μm waveguides.

3 Device Fabrication

In general, fabrication parameters for silicon photonics devices are optimized in accordance with the CMOS process lines. The components are broadly classified into two categories: (i) passive components like strip waveguides, 2D photonic crystal, DBR and grating couplers, and (ii) active components like p-i-n structure for plasma-optic phase-shifters, and microheater for thermo-optic phase-shifters. In this section, we present fabrication processes standardized for some of these integrated optical components in our labs.

3.1 Waveguide Fabrication

As mentioned earlier, waveguide is the basic building block for most of the passive and active devices in SOI platform. Waveguide on 5 μm and 2 μm SOI substrates are fabricated using photolithography (with positivetone photoresist S1813 or S1805) and subsequent dry etching process (using photoresist as etch mask), whereas waveguides fabricated with 250 nm device layer thickness are defined using e-beam lithography. Figure 5(a) and 5(b) show the waveguide fabrication process flow using photolithography and e-beam lithography, respectively.

Table 2. Optimized etching parameters for the fabrication of waveguides and some of their measured properties.

Device layer	Etching Mechanism	Etching Chemistry	Etch Rate ($\mu\text{m}/\text{min}$)	Typical etch depth (μm)	Typical surface roughness (nm)	Side-wall angle	Propagation loss (dB/cm)
5 μm	RIE	SF ₆ : Ar:: 20:20	0.35	1	10	95°	0.5
2 μm	ICP-RIE	SF ₆ : CHF ₃ :: 15:30	0.95	0.6	20-30	90°	1.3-1.5
250 nm	ICP-RIE	SF ₆ : CHF ₃ :: 5:18	0.55	0.1	10-20	90°	3.0

The fabricated waveguides are characterized in terms of surface roughness, side-wall angle, propagation loss, and mode-size, etc. Table 2 summarizes the various etching parameters optimized for the different dimensions and some typical characterization results. The 5 μm and 2 μm waveguides are cleaved or polished to prepare the end-facet for optical characterizations. Photonic wire waveguides are characterized by integrating grating couplers at the input/output ends. The mode profiles for TE polarization of 5 μm , 2 μm and photonic wire waveguides are shown in Fig 6; they are obtained by imaging the near-field distribution of guided modes at the output. It is worth mentioning here that to obtain the mode profile of the photonic wire waveguide, end-facet polishing has been carried out though grating coupler is used otherwise. The estimated mode-size of the photonic wire waveguides appears to be larger than that of theoretical prediction,

which can be attributed to diffraction limit of the imaging lens and resolution of IR camera used in our characterization setup. Besides conventional rib waveguides, we have optimized the fabrication process for 2D photonic crystal waveguides in 250-nm SOI substrate. SEM images of typical grating coupler, photonic crystal waveguide, directional coupler, and cleaved end-facet of a rib waveguide are shown in Figs 7 (a), (b), (c) and (d), respectively.

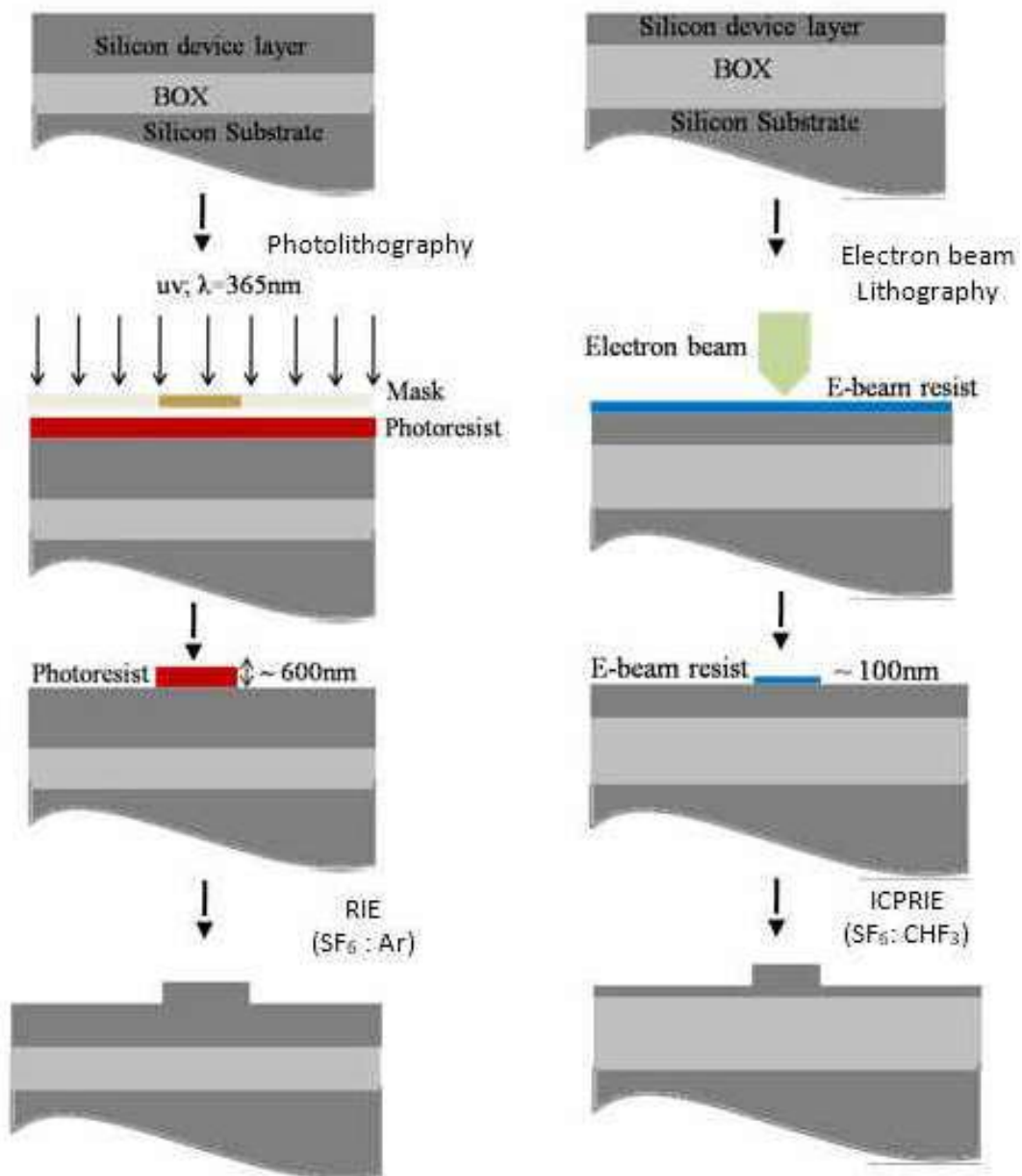
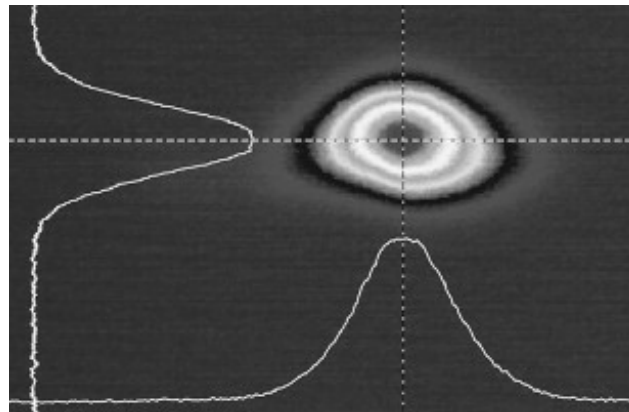
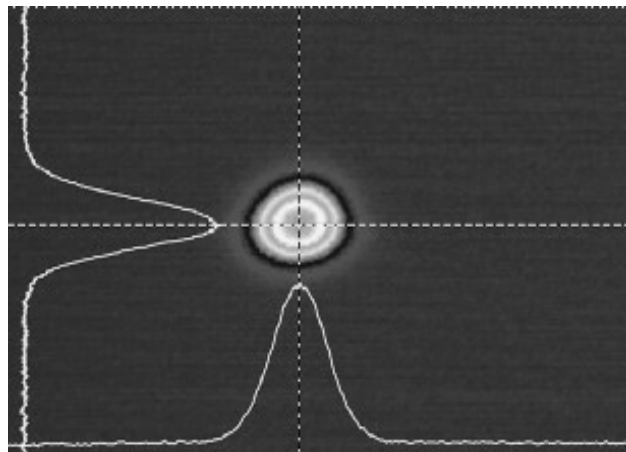


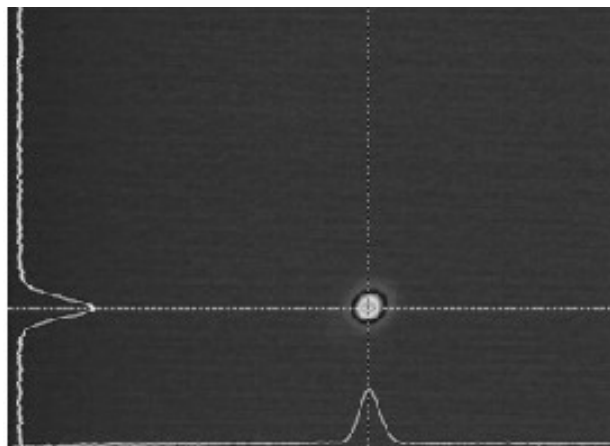
Fig 5. Fabrication process flow for waveguide defined by: (a) photolithography and (b) e-beam lithography.



(a)

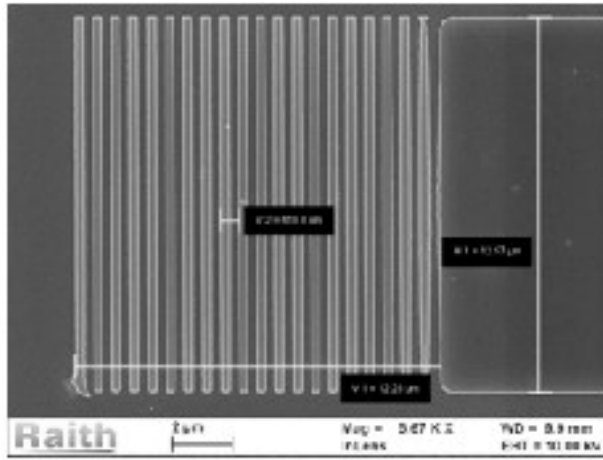


(b)

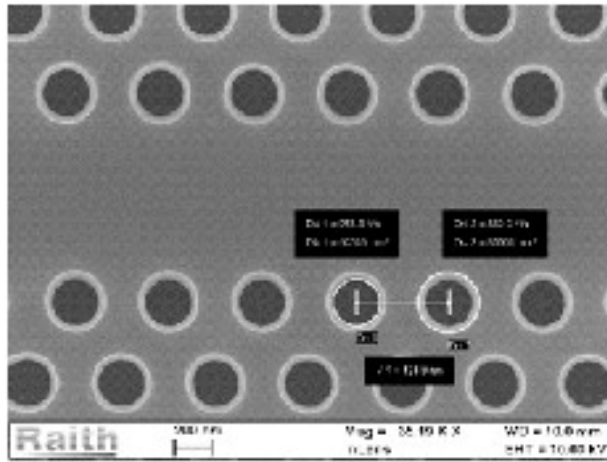


(c)

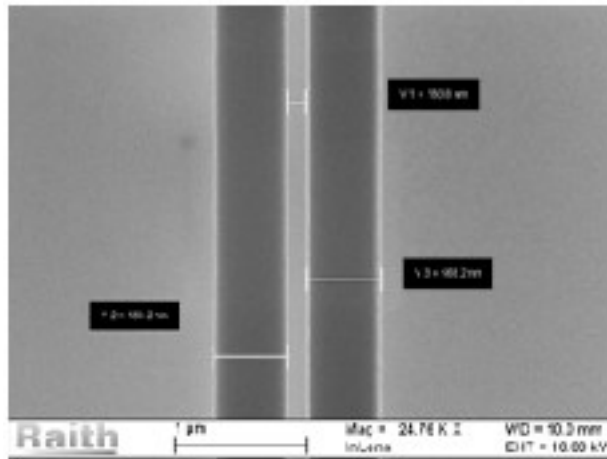
Fig 6. Measured near-field intensity distributions (TE-like mode) of single-mode waveguides fabricated with device layer thickness: (a) 5- μm , (b) 2- μm , and (c) 250-nm.



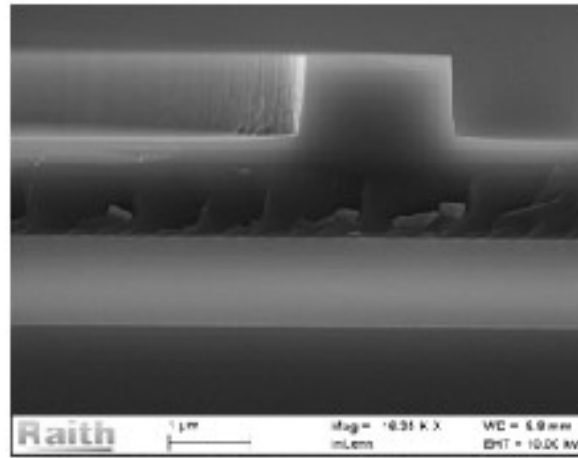
(a)



(b)



(c)



(d)

Fig 7. SEM images of fabricated devices: (a) grating coupler (250-nm SOI), (b) photonic crystal waveguide (250-nm SOI), (c) directional coupler (250-nm SOI) and (d) cleaved end-facet of waveguide (2- μ m SOI).

3.2 Fabrication of PIN diodes

The p-i-n diode is used as a high-speed active element for reconfigurable silicon photonics devices. It is usually integrated after the waveguide definition. Figure 8 shows the fabrication flow for the p-i-n diode integration with a rib waveguide in 2 μ m SOI. First, the surface layer of rib waveguide is oxidized to a thickness of \sim 500 nm using standard dry-wet-dry oxidation steps at 1000°C. A photolithography step is carried out to define oxide mask for phosphorous diffusion (n-type doping). Phosphorous dopants are sourced from the liquid POCl_3 kept at 0°C using carrier gases. Oxygen and Nitrogen. The diffusion doping is carried out for 120 minutes by maintaining the sample temperature at 850°C; which gives a junction depth of 0.2 μ m. The junction depth for phosphorus increases to \sim 1.2 μ m after all the subsequent high temperature

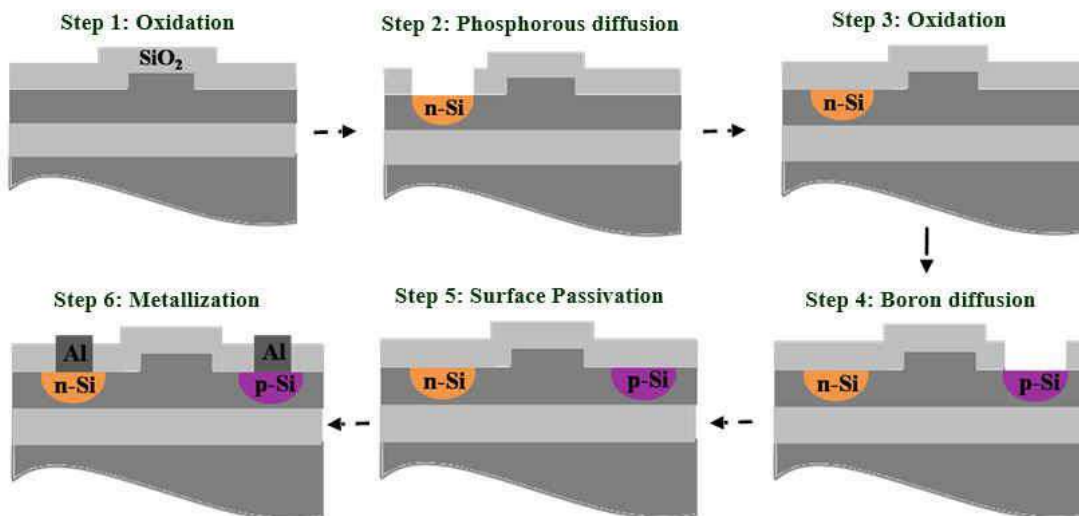


Fig 8. The fabrication process steps of a p-i-n waveguide phase-shifter.

processes of oxidation and boron diffusion. Similar steps of oxidation and photolithography are followed for Boron diffusion (p-type doping). Boron Nitride (BN1100) discs are used as the solid dopant source for diffusion at 1050°C for 15 minutes. A drive -in step is done after both the diffusion steps. A final step of oxidation is performed for surface passivation and a lithographic step to define the metal contacts. Aluminum (Al) is evaporated to form the contact pads. Typical values of dopant surface concentration and junction depth obtained after diffusion is summarized in Table 3.

Table 3. Dopant surface concentrations (extracted from sheet resistance) and estimated junction depths

Type of diffusion	Surface concentration (cm^{-3})	Junction depth (μm)
Phosphorous	4×10^{20}	1.2
Boron	4.4×10^{20}	1.3

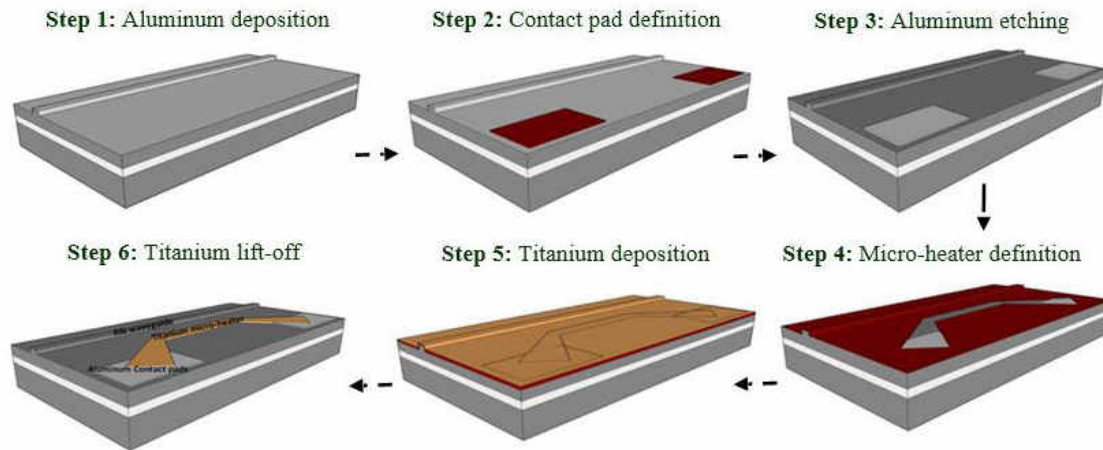


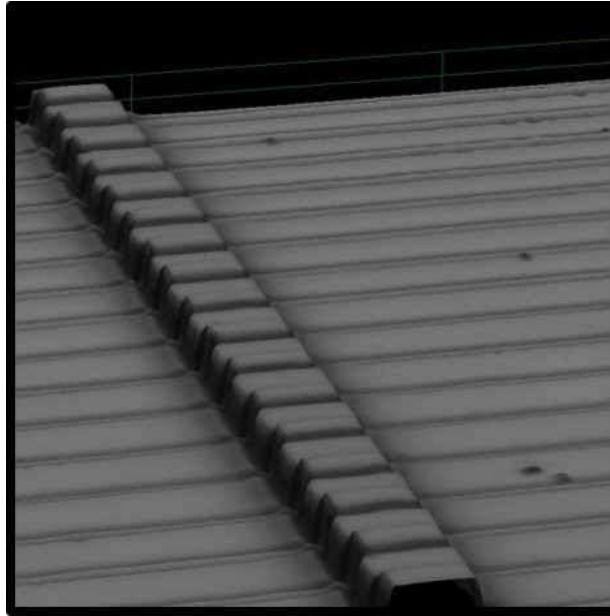
Fig 9. Fabrication process steps for an integrated optical microheater based phase-shifter.

3.3 Fabrication of microheater

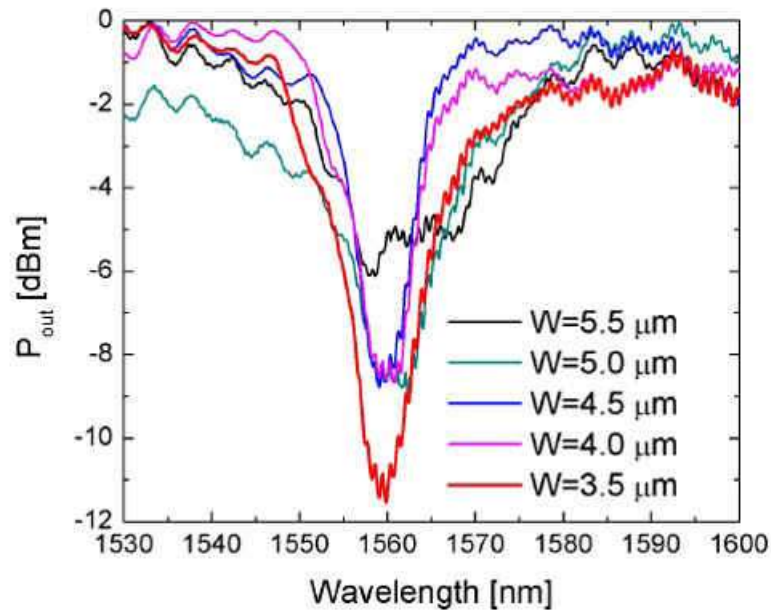
Fabrication process of integrated optical micro-heaters with single-mode rib waveguide in $2\mu\text{m}$ SOI has been optimized for thermo-optic tuning. The fabrication flow is depicted in Fig 9. Photolithographically defined titanium (Ti) stripe (width $\sim 2\text{-}3\ \mu\text{m}$, thickness $\sim 130\ \text{nm}$, lengths $50\text{-}200\ \mu\text{m}$) close to waveguide (at a $3\ \mu\text{m}$ distance from the waveguide) is used as heater element and Al pads are used for electrical contact. The estimated line resistance for a $2\text{-}\mu\text{m}$ -wide heater is $20\ \Omega/\mu\text{m}$ and for $3\text{-}\mu\text{m}$ -wide heaters is $13\ \Omega/\mu\text{m}$.

4 Devices with $5\ \mu\text{m}$ SOI

Integrated optical devices with relatively large cross-section waveguides in SOI substrate do not have any requirement of stringent lithographic definitions [16]. Moreover, one can easily characterize the fabricated devices using free-space optics and can be pigtailed with standard single-mode fibers for system-level applications. Devices like eleventh order DBR filter, multimode interference (MMI) based 1×8 power splitter, 2×2 directional coupler for 3-dB power splitting, Mach-Zehnder interferometer based ITU channel interleaver, variable optical attenuator and Mach-Zehnder switch, etc. have been designed and fabricated using SOI substrates with a device layer thickness of $\sim 5\ \mu\text{m}$. Their design parameters, working principle and characterization results are discussed briefly in this section.



(a)



(b)

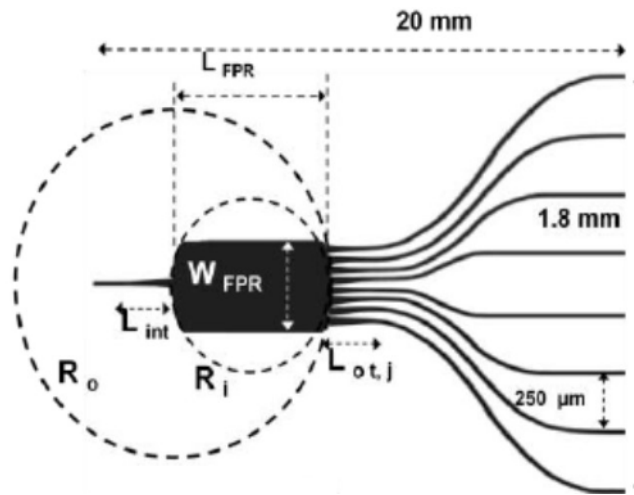
Fig 10. (a) The confocal microscopic image of an 11th order DBR grating integrated with single-mode waveguide in a SOI substrate with 5 μm device layer thickness; (b) The transmission characteristics (TE-pol) of the fabricated DBR with grating period of $\Lambda = 2.6 \mu\text{m}$, modulation depth $\Delta h = 260 \text{ nm}$, LDBR = 5.2 mm, waveguide height $H = 5 \mu\text{m}$, slab height $h = 3.8 \mu\text{m}$ and the waveguide width W varied from 5.5 μm to 3.5 μm. The spectrum is normalized with the transmission spectrum of straight waveguide and for a peak output power of 1 mW.

4.1 DBR Filter

Grating structures are widely used for developing integrated optical devices like couplers, filters, (de-) multiplexers, interleavers, Distributed Bragg Reflector (DBR) cavities, laser sources, etc. Because of the huge prospects of CMOS compatible photonic devices in SOI platform, there have been great interest to develop efficient DBR structures with single-mode silicon waveguides. In order to realize first order DBRs, a periodicity of $\Lambda \sim 280$ nm (smallest feature size ~ 140 nm) is required to obtain a reflection peak at $\lambda \sim 1550$ nm. The fabrication of such sub-micron grating structures requires stringent process control. Therefore, we have demonstrated grating structures with a feature size ~ 1.3 μm (2.4 $\mu\text{m} \leq \Lambda \leq 2.6$ μm) to be used as integrated optical DBRs with $\lambda_{\text{Bragg}} \sim 1550$ nm (see Fig 10). The fabrication was carried out using two step photolithography and RIE processes. The first step was used to define DBR structures (duty cycle: 50%, corrugation depth: ~ 250 nm), whereas the second step was to define single-mode rib waveguides (rib height: 5 μm , slab height: 3.8 μm , width: 3.0 $\mu\text{m} \leq W \leq 5.5$ μm). After fabrication, the waveguide end-facets were polished to a roughness of < 200 nm before they were taken for characterizations using an end-fire waveguide coupling set-up. The characterization results of the fabricated DBRs show a reflection of $> 90\%$ and FWHM ~ 3.3 nm (estimated from transmission spectrum) for a grating length of 5.2 mm for TE polarization.

4.2 MMI based 1×8 Power Splitter

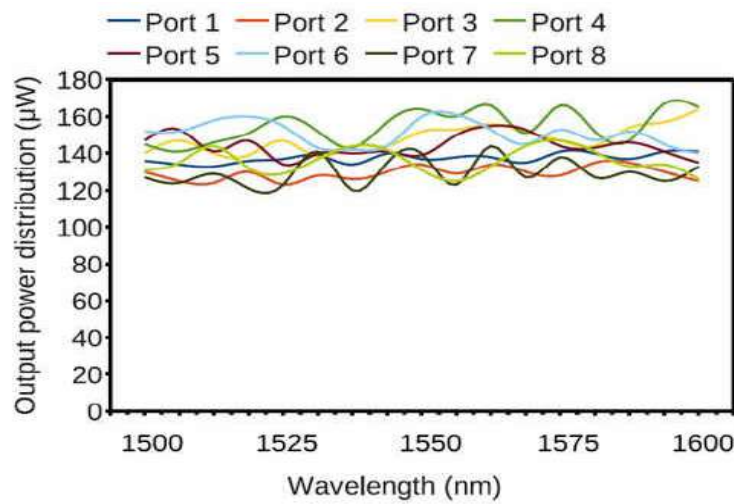
Integrated optical power splitter is an important component in passive/active optical network systems. Such power splitters are mostly being manufactured in silica-on-silicon platform using planar lightwave circuit technologies. We have demonstrated multimode interference (MMI) based integrated optical 1×8 power splitter in SOI substrate with large cross-section single-mode input/output waveguides. The device basically consists of one single mode input waveguide, eight single mode output waveguides and a planar waveguide (MMI region) in between. The device parameters were optimized by BPM simulation results and fine-tuned based on preliminary experimental investigations. While optimizing the design parameters, care was taken to minimize the wavelength / polarization dependencies, insertion loss, excess loss and throughput power non uniformity among the output waveguides. The device (dimension ~ 20 mm \times 2 mm) has also been designed such that it could be pigtailed with standard single mode fibers. Typical spot-size of the guided fundamental mode in these waveguides is estimated to be ~ 7.2 $\mu\text{m} \times 4.6$ μm – nearly equivalent to that of standard single-mode fiber operating at $\lambda \sim 1550$ nm. The fabricated devices have been characterized in terms of excess loss, insertion loss, non-uniformity in throughput powers and polarization / wavelength dependencies (1520 nm $< \lambda < 1600$ nm). The devices were found to be nearly wavelength / polarization



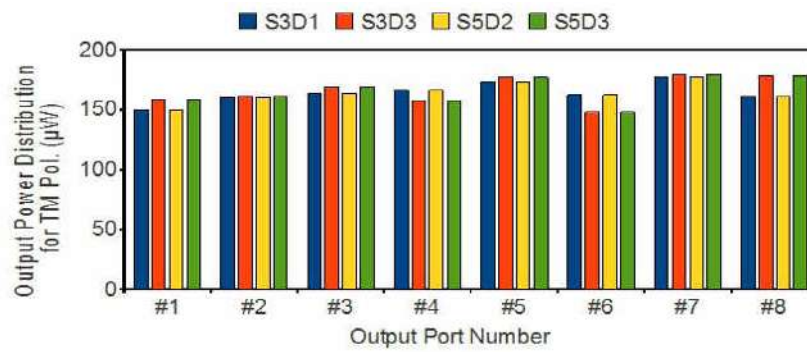
(a)



(b)



(c)



(d)

Fig 11. (a) The scheme 1×8 power splitter designed with $5\text{-}\mu\text{m}$ device layer thickness; (b) Photograph of a fiber pigtailed and packaged 1×8 power splitter. FPR - free propagation region, R_i and R_o are the radii of the Rowland and grating circles, respectively; (c) Wavelength dependent transmission characteristics (TM-pol.) of a packaged device; (d) The transmitter power profiles of four different devices (S3D1, S3D3, S5D2, S5D3) for TM-polarization at an operating wavelength $\lambda = 1550\text{ nm}$ ($P_{in} = 5\text{ mW}$). The devices are found to be nearly polarization independent.

insensitive. By analyzing the experimental results, we have observed typical insertion loss of 15 dB with power non-uniformity of 0.7 dB among output ports and excess loss of 7 dB. A prototype (1×8) power splitter have also been pigtailed with standard single mode fiber and packaged. The corresponding characterization results suggest that such power splitters can be potentially useful in passive/active optical networks operating in the communication window of $\lambda \sim 1550$ nm and it can be scalable for the realization of 1×16, 1×32, 1×64, etc. power splitters for the use in fiber to the home/office (FTTH/FTTX) networks.

4.3 ITU Channel Interleaver

Dense Wavelength Division Multiplexing (DWDM) has recently attracted much interest in-order to meet the growing need for higher channel capacity over fiber-optic communication links. This demand has led International Telecom Union (ITU) to repeatedly reduce and re-define channel spacing in the orders of 100-, 50-, 25- GHz. As a result, there is an intense need for channel interleaver devices in order to improve the performance at transmitter / receiver ends.

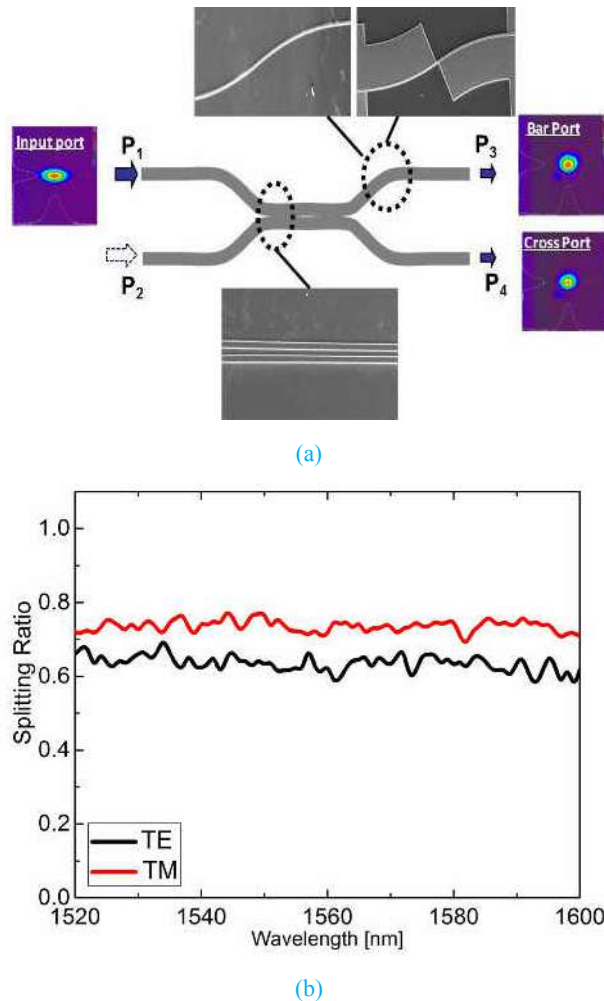
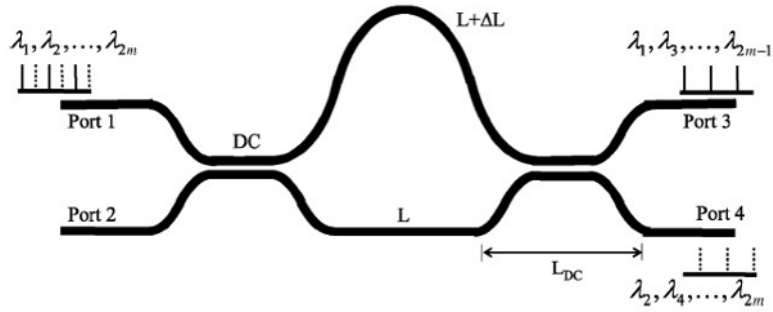


Fig 12. (a) Schematic representation of a 2×2 directional coupler along with fabricated features (SEM images) of a coupled waveguide section, S-bends with both-sided and one-sided slab, (b) Wavelength dependent transmission (power splitting ratio) at one of the output port for both TE and TM polarizations.

Table 4. Final design parameters for 100 GHz ITU channel interleaver fabricated with 5 μm SOI

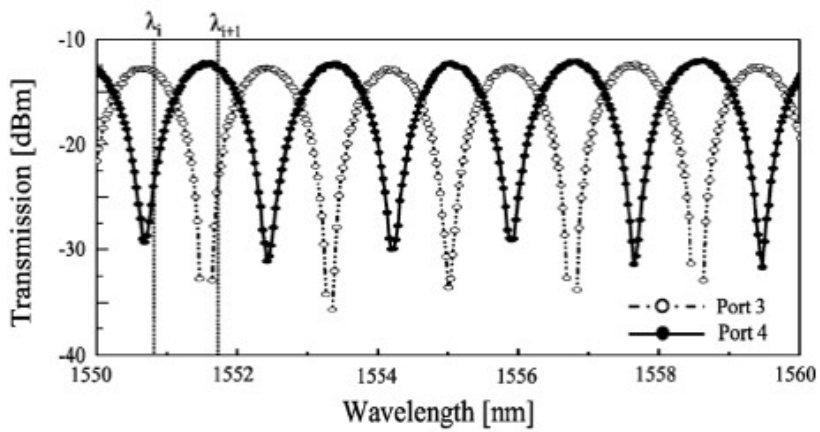
Waveguide width = 5 μm	Waveguide spacing for the directional couplers = 2.5 μm
Rib (slab) height = 1.8 μm (3.2 μm)	Length of directional couplers = 1400 μm
Waveguide bending radius = 15000 μm	$\Delta L = 415.4 \mu\text{m}$
Total Device length = 29 mm	Operation band = C and L



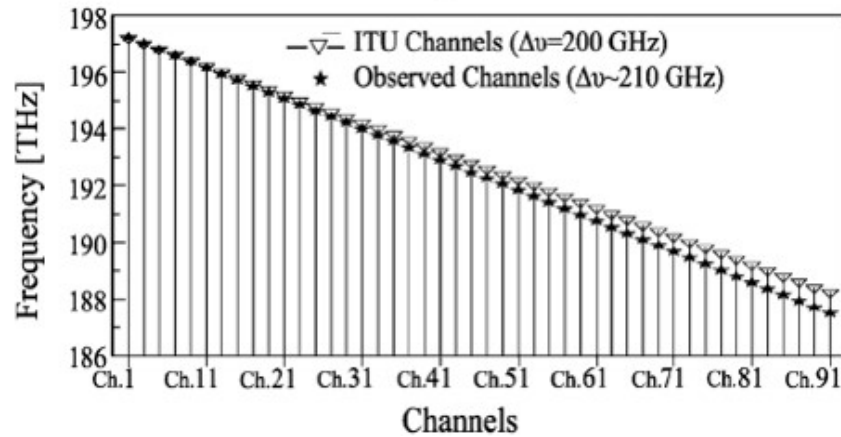
(a)



(b)



(c)



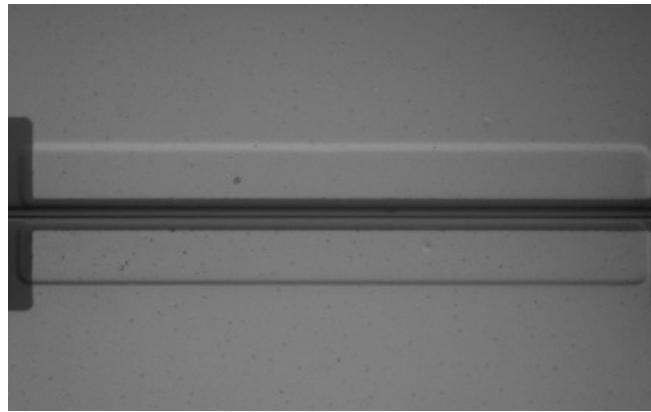
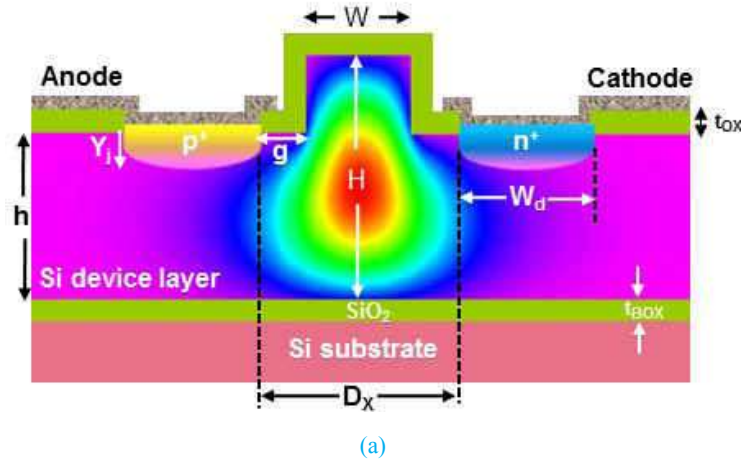
(d)

Fig 13. (a) Scheme of an unbalanced Mach-Zehnder Interferometer (MZI) used to design the 100 GHz ITU channel interleaver in SOI platform with 5 μm device layer thickness. DC - directional coupler (for 3-dB power splitting) ; (b) Fiber pigtailed and packaged interleaver; (c) Wavelength dependent transmission at both the output ports for TE polarization; (d) Experimentally observed channel positions at bar port and comparison to that ITU channels.

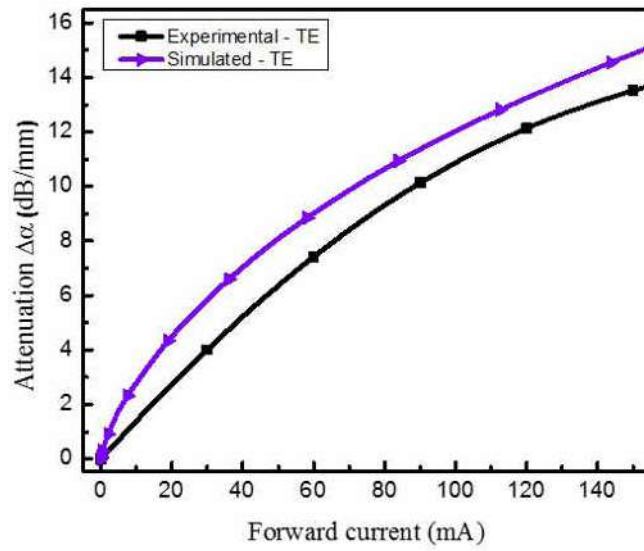
An integrated optical interleaver device in SOI platform with 5- μm waveguides was demonstrated for 100 GHz channel spacing. It is basically an unbalanced Mach-Zehnder Interferometer (MZI) designed by cascading two identical DCs. The length of DCs is adjusted for 3-dB power splitting for a wide-range of wavelengths (see Fig 12). The optimized values of critical design parameters have been given in Table 4. The devices were fabricated with optimized design parameters, and characterized in terms of insertion loss, wavelength / polarization dependencies and inter-channel extinction over $\lambda = 1520$ to 1600 nm. Some of the 2×2 prototype devices have been fiber pigtailed, and packaged. Typical inter channel extinction is measured to be more than 15 dB with 3 dB channel passband of ~ 40 GHz (see Fig 13 (b)).

4.4 Variable optical attenuator and Mach-Zehnder switch

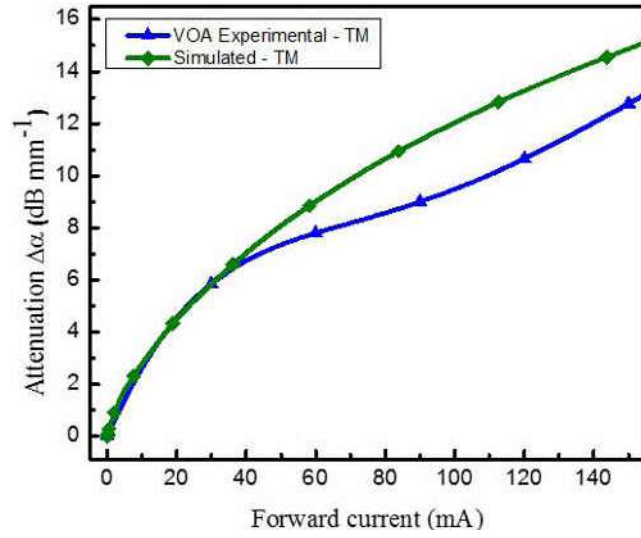
Design of diffusion doped p-i-n structures with large cross-section ($\sim 25 \mu\text{m}^2$) single mode rib waveguide structures on SOI platform have been studied for the demonstration of variable optical attenuator (VOA) and MZI Switch. RSoft FEMSIM and MEDICI simulation tools were used for the final design of single-mode p-i-n waveguide section. Since the forward biased p-i-n waveguide offers simultaneous reduction of refractive index and increment in attenuation because of plasma dispersion effect, we have optimized its length of 230 μm for the fabrication of VOAs and MZI switches. The static modulation characteristics of these devices were experimentally studied and typical results shown in Figs 14 and 15, respectively. Typical attenuation of a VOA was measured to be 2.0 (3.6) dB/mm for TE (TM) - polarized light ($\lambda \sim 1550$ nm) at a forward current of 15 mA. We must emphasize that the experimentally observed attenuation characteristics were found to be slightly deviated from the simulated results, which may be attributed to non-ideal waveguide side-walls and hence deviations in various parameters including guided mode profiles. The extinction ratio of the modulator was found to be 12.4 dB and 12 dB for TE and TM polarizations, respectively. Transient response of the fabricated MZI switches were obtained by modulating the bias voltage with a rectangular pulse of duration 500 ns (repetition rate of 1 MHz). The estimated rise-time and fall-time of a MZI switch were recorded as 61 ns and 159 ns, respectively.



(b)

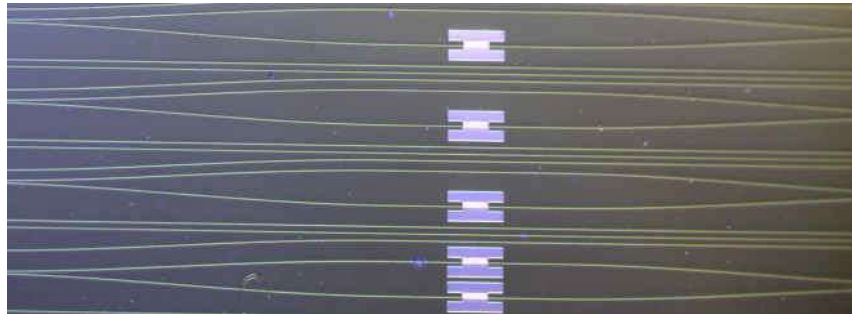


(c)

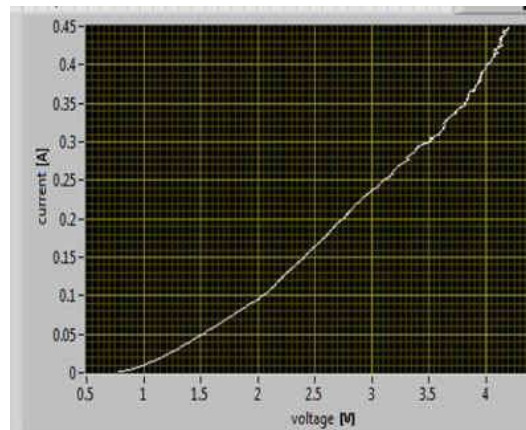


(d)

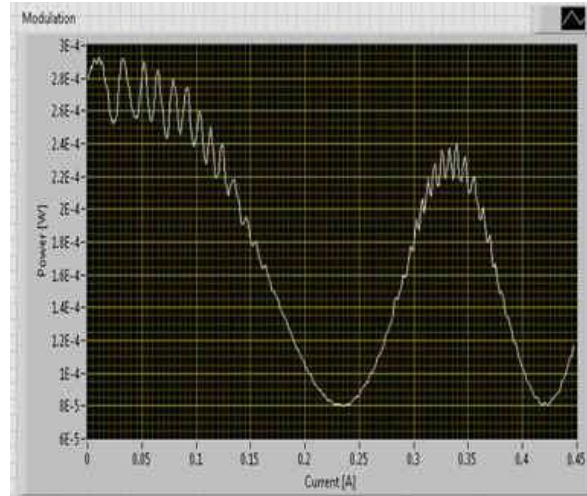
Fig 14. (a) Schematic representation of cross-sectional p-i-n waveguide phase-shifter/variable optical attenuator along with simulated guided mode profile for TE-polarization ($\lambda = 1550$ nm); (b) Microscopic image showing top view of a fabricated variable optical attenuator; (c) Attenuation characteristics for TE -polarization; (d) Attenuation characteristics for TM -polarization



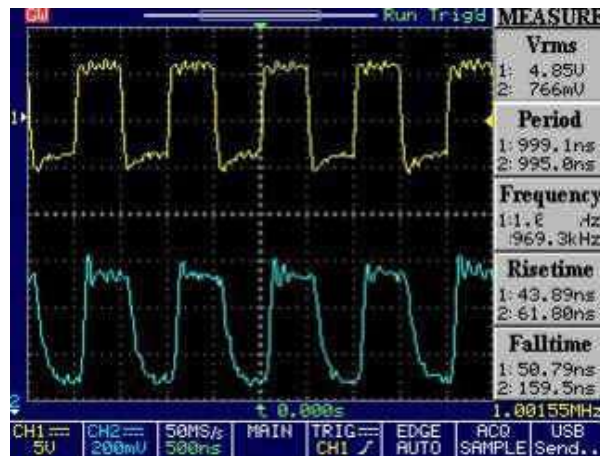
(a)



(b)



(c)

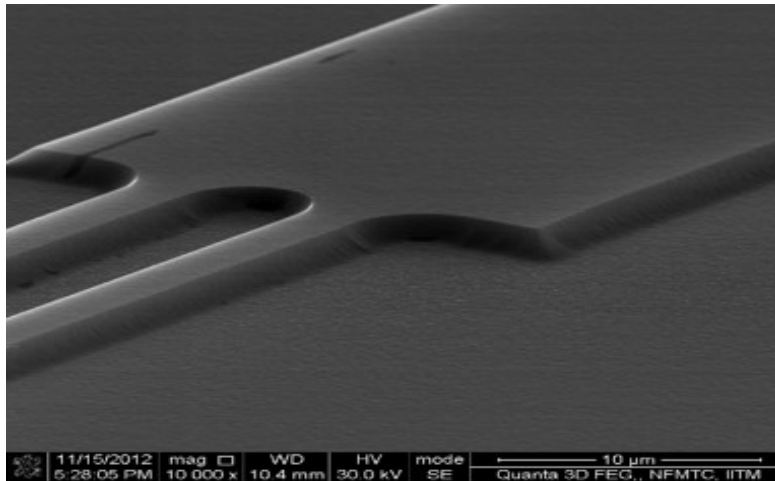


(d)

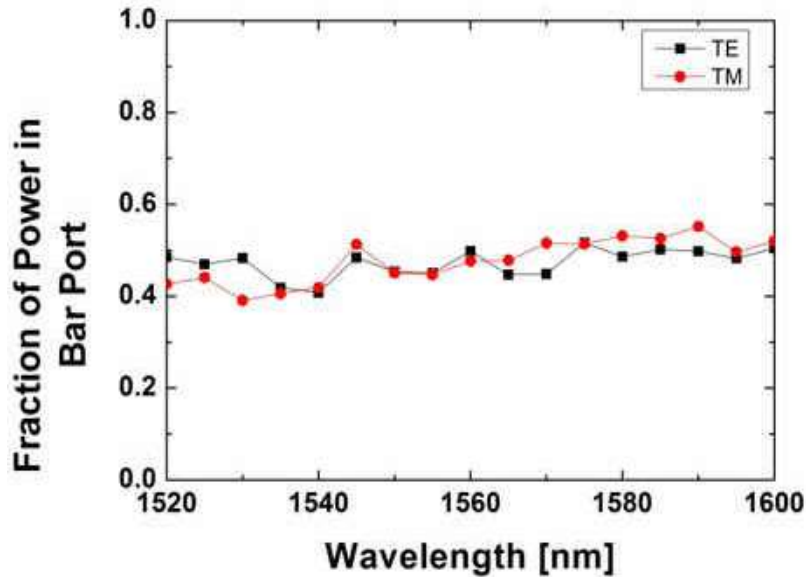
Fig 15. (a) Microscopic image of fabricated MZI switches; (b) I-V characteristics; (c) Modulated light output as a function of forward current; (d) Switching performance with rectangular input pulse captured by a digital storage oscilloscope; blue (yellow) color represent modulated optical output (bias voltage).

5 Devices with 2- μ m SOI

As we understand from theoretical simulation, single-mode waveguide design in a SOI substrate with 2- μ m device layer thickness offers nearly polarization independent, lower propagation loss, and necessary dispersion engineering for nonlinear phase matching as well as higher chip to fiber light coupling efficiency using commercially available lensed fiber. In this section, we present briefly the performances of some devices like MMI based 3-dB power splitter, wavelength independent ITU channel interleaver, large volume microring resonator and thermo-optic phase shifter which were fabricated in 2- μ m SOI platform.



(a)



(b)

Fig 16. (a) SEM image showing the junction points of two input/output waveguides and the multimode waveguide section of a 2×2 MMI based 3-dB power splitter, (b) Wavelength dependent transmission characteristics of a typical MMI based 3-dB power splitter fabricated with $2 \mu\text{m}$ SOI.

5.1 MMI based 3-dB power splitter

The design principle and an optimized set of parameter values for a typical 2×2 MMI based 3-dB power splitter with $2 \mu\text{m}$ SOI have been discussed earlier. The SEM image of such a fabricated device is shown in Fig 16(a). The device was designed to operate at $\lambda \sim 1550 \text{ nm}$ for both TE- and TM-like guided modes. As expected, the wavelength dependent transmission characteristics (see Fig 16(b)) also exhibit nearly polarization independent 3-dB power splitting over a broad wavelength of operation (experimental results shown for C+L bands).

5.2 Compact ITU Channel Interleaver

Following successful demonstration of dispersion-free ITU channel interleaver in 5 μm SOI [20], we explored a compact design of asymmetric MZI in 2 μm platform (see Fig 17) [24]. In contrast to the

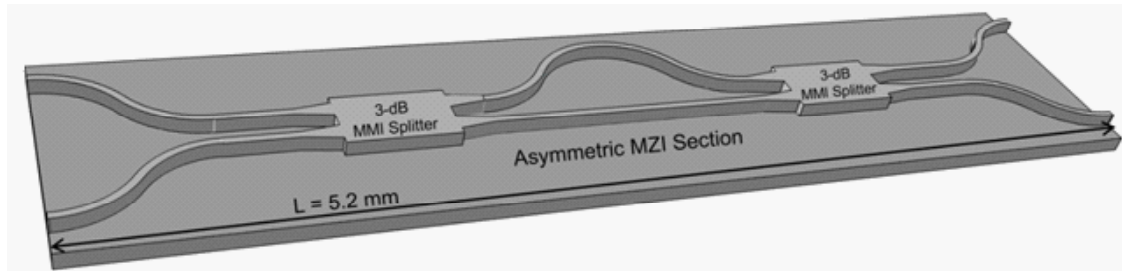


Fig 17. Schematic 3D view of compact interleaver designed with 2- μm SOI

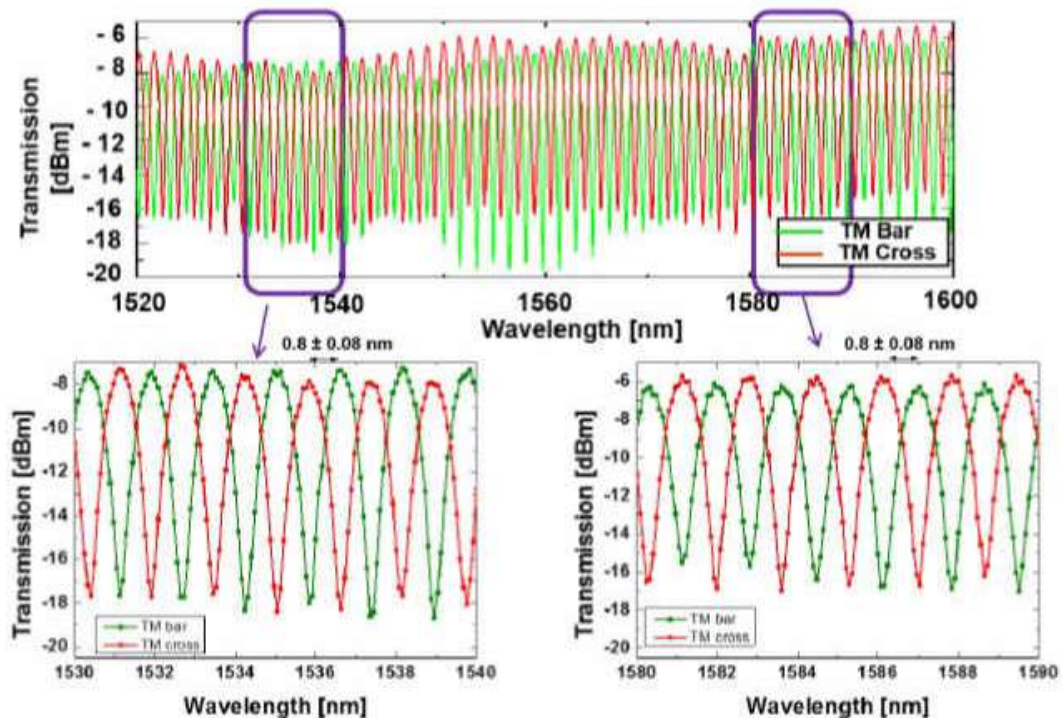


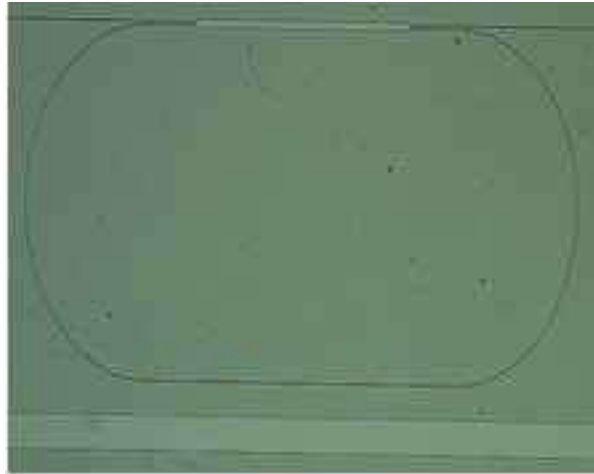
Fig 18. Normalized transmission characteristics (shown for TM polarization) exhibiting a nearly uniform extinction over wide-band of operation ($1520 \text{ nm} < \lambda < 1600 \text{ nm}$).

design of DC based interleaver in 5 μm SOI discussed earlier, two MMI based 3-dB couplers were cascaded to construct the 2×2 asymmetric MZI. The arm lengths of the MZI are 3037 μm and 3450 μm , respectively. The differential arm length of $\Delta L \sim 412 \mu\text{m}$ has been added in the upper arm by means of S-bends (loss-less design), specifically to obtain alternate ITU channels (spaced by 100 GHz) transmission peaks at both the output ports alternatively. The entire device footprint is $\sim 0.8 \text{ mm} \times 5.2 \text{ mm}$ ($W \times L$). The characterization results represented in Fig 18 show that the device could separate alternate ITU channels into two output ports.

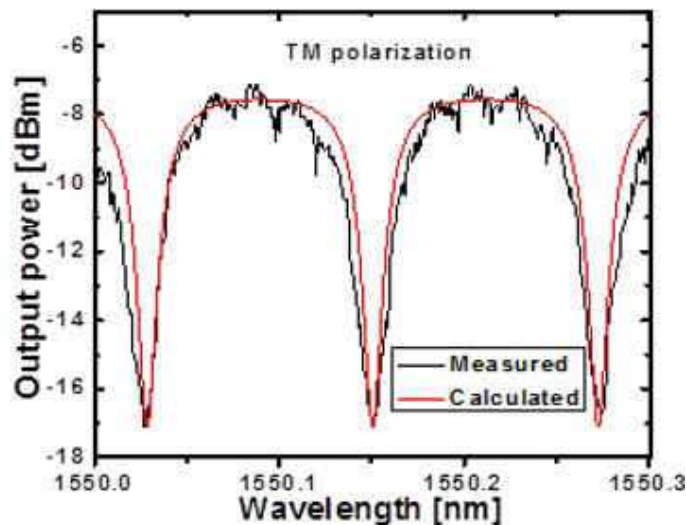
We also observe a uniform channel extinction of ~ 15 dB with a 3-dB bandwidth of ~ 100 GHz for either polarization at the output ports over the wavelength range of 1520 nm to 1600 nm. The devices show nearly dispersion-free response and polarization-independent extinction over a wide wavelength range (C+L optical band).

5.3 Large-volume Ring Resonator

Ring resonator is most versatile fundamental building block for integrated optics applications. While a passive waveguide ring resonator characteristically exhibits a notch filter, integration of an active element (thermo-optic or plasma-optic phase-shifter) enables tunable filtering, modulation, and switching. An extensive review is available on various applications and functionalities using a ring resonator [44]. In general, microring resonators are fabricated with photonic wire waveguide with tightly confined mode,



(a)



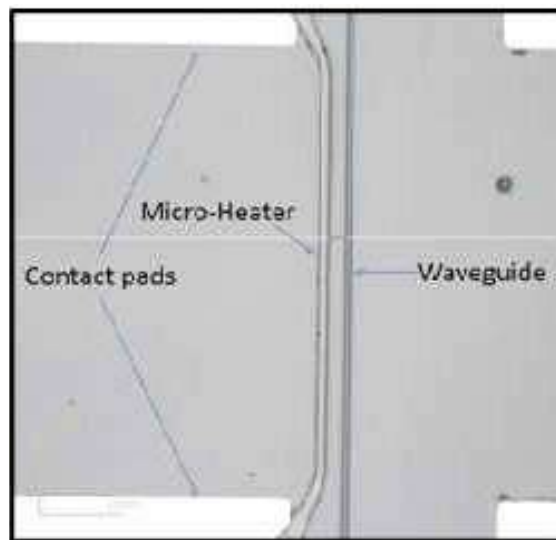
(b)

Fig 19. (a) Microscopic top view of ring resonator, (b) Transmission characteristics of ring resonator.

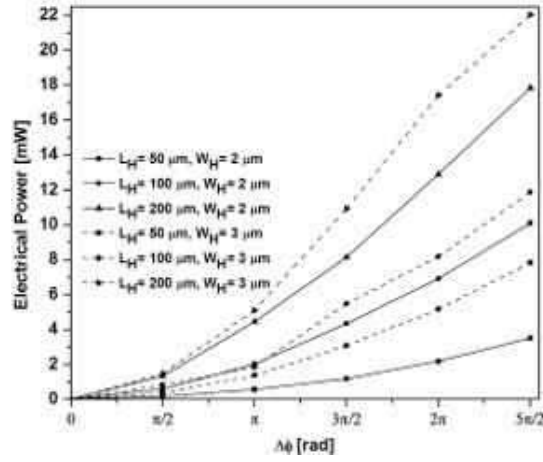
especially to reduce bend-induced loss as well as simultaneously to obtain large free spectral range (FSR). We designed and fabricated a relatively large volume ring resonator of race track type with MMI coupler for feeding power into the ring waveguide with 2- μm single-mode waveguides. The device foot print is $\sim 1.5 \times 1.5$ mm, with ring radius of 500 μm and MMI coupler length of 1.25 mm. Figure 19 (a) shows the microscopic view of the fabricated device. Transmission characteristics are shown in Fig 19 (b). The device shows an extinction of ~ 10 dB and FSR of 122 pm. The Q-value is estimated to be large $\sim 9.6 \times 10^4$; which is a clear evidence of lower round-trip loss even for large volume ring resonator. Such high Q-value ring resonator device may be useful in sensing applications.

5.4 Thermo-optic Switch

The presence of strong thermo-optic effect in silicon ($dn/dT \sim 2 \times 10^{-4}/\text{K}$), enables large scale integration of reconfigurable optical systems viz. routers [45-46], couplers [47], filters [48], delay lines [49], switches [50], etc. Integrated optical micro-heaters can be used for local reconfiguration/correction of phase-sensitive devices via thermo-optic effect. However, high thermal sensitivity of resonance devices ($d\lambda_r/dT \sim 100$ pm/K) leads to thermal crosstalk, especially for densely packed large-scale integrated optical circuits in SOI platform. It is therefore, important to investigate the temperature distribution and effective control of thermo-optic phase-shift by a micro-heater integrated with waveguide structures [51]. We fabricated waveguides integrated with titanium micro-heater placed adjacent to waveguide as discussed in section 3. The micro-heaters were placed at a 3 μm separation from the base of the rib waveguide to avoid optical losses. There were two sets of micro-heaters with width 2 μm and 3 μm . The lengths were varied from 50 μm to 200 μm . The estimated resistance/length for 2 μm width heaters was 20 $\Omega/\mu\text{m}$ and for 3 μm width heaters was 13 $\Omega/\mu\text{m}$. Figure 20 (a) shows the microscopic image of heater. The device was polished using diamond lapping film for optical and electrical characterization. Figure 20 (b) shows the thermal tuning characteristics for different lengths of heater and separation from the waveguide edge. Fabry-Perot modulation technique was used to extract the effective thermo-optic phase-shifts and is presented in Fig 21 (a). Transient response was also recorded by applying a square wave as shown in Fig 21 (b). A typical thermo-optic phase tuning efficiency of $\sim 0.9\pi$ rad/mW and a response time of ~ 7 μs were recorded for a heater of length of 50 μm and width of 2 μm integrated with a waveguide of length ~ 20 mm.

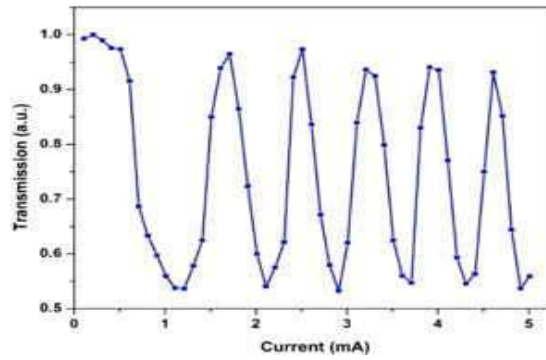


(a)

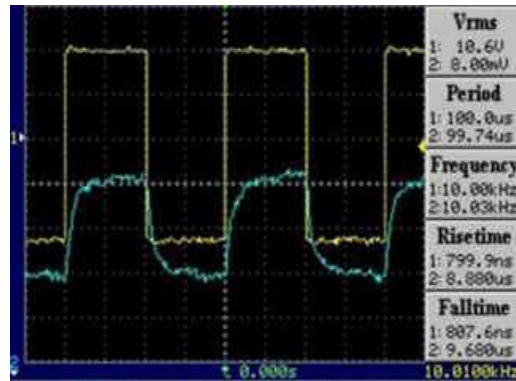


(b)

Fig 20. (a) Confocal micrograph of fabricated micro-heaters integrated with single mode rib waveguides, (b) effective electrical power (P_{eff}) versus induced phase change $\Delta\phi$ in the waveguide for heater width $W_H = 2 \mu m$ (solid line) and $W_H = 3 \mu m$ (dotted line), and different heater length L_H viz. $50 \mu m$, $100 \mu m$, $200 \mu m$ for TE polarized light.



(a)



(b)

Fig 21. (a) Fabry-Perot response with thermal tuning; (b) Transient response: yellow trace - driving electrical signal, blue trace - optical output.

6 Devices with 250-nm SOI

Devices with 250-nm SOI can be fabricated with ultra-compact designs because of tightly confined waveguide modes. The devices are fabricated with input/output grating couplers (see Fig 7(a)) and can be easily characterized by fiber-optic probe station. Photonic wire waveguides fabricated in our labs exhibit an average propagation loss of ~ 3 dB/cm for TE-like guided modes. Recently, two important integrated optical devices namely, (i) DBR filter and (ii) microring resonator have been successfully demonstrated in our labs. Their performance characteristics are discussed in this section.

6.1 Narrow-line-width DBR Filter

The side-wall DBR gratings with a period of 290 nm and lengths up to $750 \mu\text{m}$ have been integrated with photonic wire rib waveguides ($W = 560$ nm, $H = 250$ nm, and $h = 150$ nm). SEM image of a single-mode

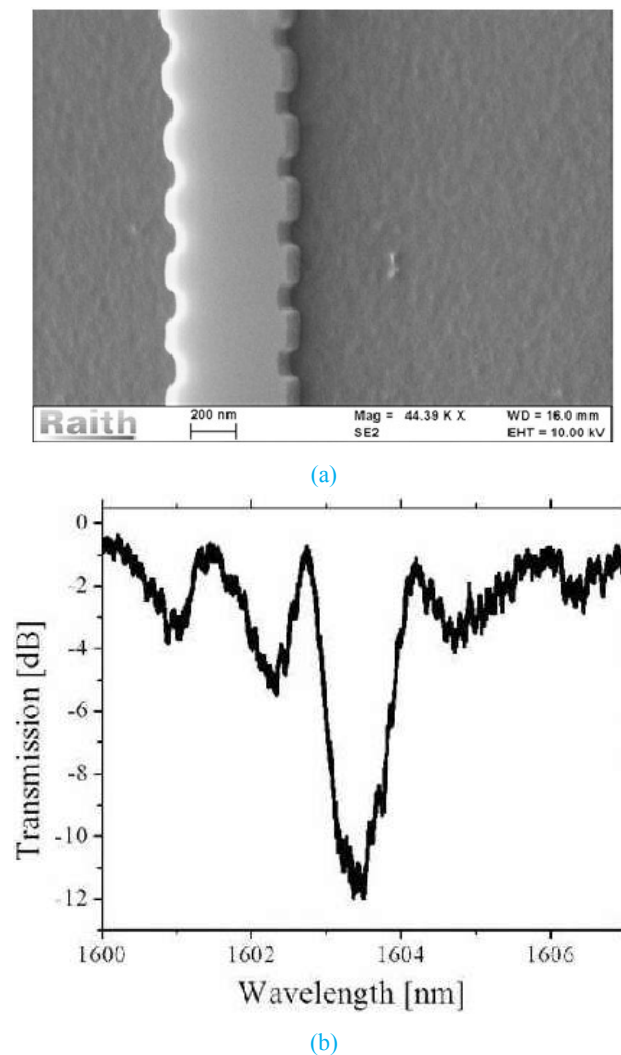


Fig 22. (a) SEM image of the side wall grating fabricated in SOI photonic wire using e-beam lithography (b) Transmission characteristics of $500 \mu\text{m}$ long DBR structure in SOI.

waveguide with side-wall grating (modulation $\Delta W = 50$ nm) and the transmission characteristics of a 500 μm long DBR filter are shown in Fig 22 (a) and 22 (b), respectively. A transmission dip of more than 10 dB at $\lambda_{\text{Bragg}} = 1603.5$ nm has been observed with an estimated FWHM of ~ 1 nm. Insertion loss of DBR filters fabricated in our labs is extracted to be ~ 2 dB for the guidance of TE-like fundamental mode.

6.2 Microring Resonator

Microring resonators were fabricated with single-mode waveguides ($W = 550$ nm, $H = 250$ nm, and $h = 100$ -150 nm) supporting only the TE-like guided modes. The ring radius was varied from 10 - 200 μm to study bend-induced waveguide loss, group index of the guided mode, effective free spectral range, extinction ratio, Q-value etc. All these parameters are extracted from the transmission characteristics in all-pass filter configuration using fiber-optic probe station. As the bus and ring waveguides are evanescently coupled, the length of the coupled region (LDC) and gap (s) between them are the deciding parameters for coupling strength between the bus and ring (for a given set of waveguide parameters). We have optimized the e-beam lithography process to control the s value ~ 100 nm. SEM image of a fabricated microring resonator is shown in Fig 23 (a) along with a magnified SEM image of DC region in Fig 23 (b). Typical transmission characteristics of a microring resonator is shown in Fig 24. The FSR and quality factor of this device is measured to be ~ 0.89 nm and 141,000, respectively.

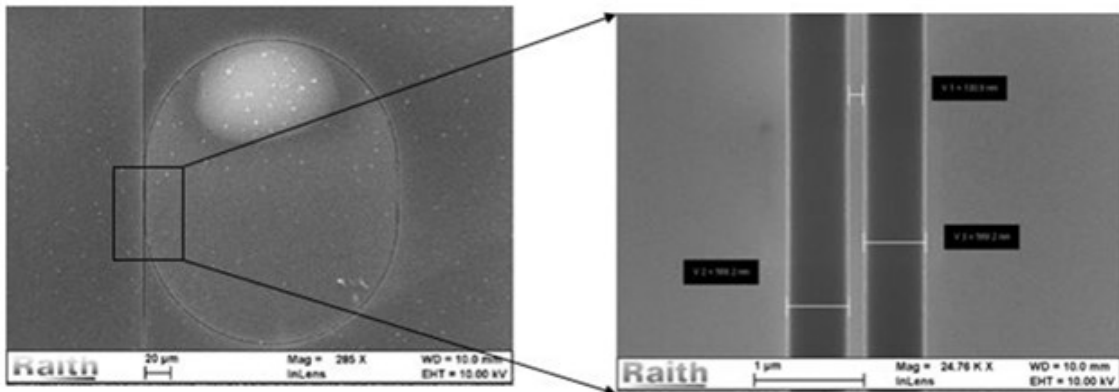


Fig 23 (a). SEM image of microring resonator, and (b) zoomed SEM image of directional coupler used in microring resonator.

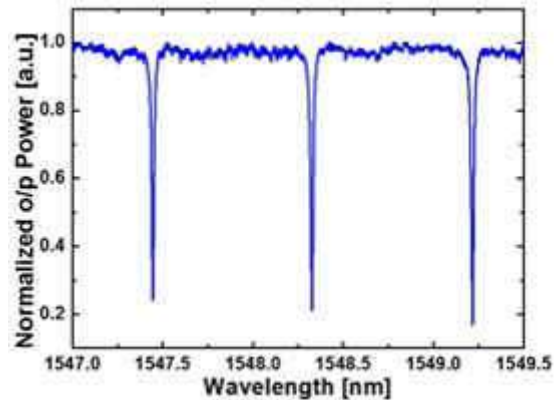


Fig 24. Transmission characteristics of a typical microring resonator fabricated on 250 nm SOI for TE polarized mode.

7 Conclusions

The objective of this article is to highlight the silicon photonics research activities carried out during last ten years in Integrated Optoelectronics Lab, IIT Madras, India. It is indeed a difficult task but we tried to elaborate our research activities as much as possible. However, the readers will definitely get a flavor of the *state-of-art* silicon photonics technology and get to know how we have achieved a little success in this area starting right from the scratch. Our silicon photonics research has been evolved from 5- μm waveguide technology to submicron or photonic wire waveguide technology. We have also explored the integration of active elements like p-i-n waveguide phase-shifter and micro-heaters for modulators/switches. Many of our recent application oriented recent research works include waveguide surface trimming, adiabatic spot-size converter, multiple-input-multiple-output waveguide platform, arrayed waveguide grating, razor-edge filter and ring resonator based wide-range refractive index sensing, etc. Some of these results have been already published or will be published in course of time.

Acknowledgments

We thankfully acknowledge following funding agencies for supporting silicon photonics research at IIT Madras.

1. DeitY, Govt. of India for the funds to establish Centre for NEMS and Nanophotonics (CNNP) at IIT Madras.
2. IRDE/DRDO, Govt. of India for the project “Silicon Nanophotonics - technology development, novel device design, fabrication and characterization”
3. DST, Govt. of India for the projects, “Development of passive integrated photonic components in SOI platform” and “Experimental demonstration and modelling of SOI based p-i-n/p-n phase-shifters and variable optical attenuators with submicron waveguides”.
4. DIT, Govt. of India for the project, “Development of integrated optical single channel add-drop multiplexer (SCADM) in SOI platform for fiber optic communication systems”
5. RCI, Hyderabad for the project, “SOI integrated optical chip for sensor applications”.

References

1. Goodman J W, Leonberger F I, Kung S Y, Athale R A, Optical interconnections for VLSI systems, *Proc IEEE*, 72(1984)850-866.
2. Miller D A B, Optical interconnects to silicon, *IEEE JSTQE*, 6(2000)1312-1317.
3. Young I A, Mohammed E, Liao J T S, Kern A M, Palermo S, Block B A, Reshotko M R, Chang P L D, Optical I/O technology for tera-scale computing, *IEEE J Solid State Circuits*, 45(2010)235-248.
4. Koehl S, Liu A, Paniccia M, Integrated Silicon Photonics: Harnessing the data explosion, *OSA Opt Photon News*, 22(2011)24-29.
5. Beausoleil R G, Large-scale integrated photonics for high-performance interconnects, *ACM JETC*, 7(2011)6:1-6:54; doi: 10.1145/1970406.1970408
6. Sun C, Wade M T, Lee Y, Orcutt J S, Alloatti L, Georgas M S, Waterman A S, Shainline J M, Avizienis R R, in S, Moss B R, Kumar R, Pavanello F, Atabaki A H, Cook H M, Ou A J, Leu J C, Chen Yu-Hsin, Ram R J, Popović M A, Stojanović V M, Single-chip microprocessor that communicates directly using light, *Nature*, 528(2015)534-538.
7. Bowers J, Liang D, Fang A, Park H, Jones R, Paniccia M, Hybrid Silicon lasers: the final frontiers to integrated computing, *OSA Opt Photon News*, 21(2010)28-33.
8. Michel J, Liu J, Kimerling L C, High-performance Ge-on-Si photodetector, *Nature Photonics*, 4(2010)527-534.
9. Thomson D J, Reed G T, Silicon modulators based on free carrier concentration variations, *Hand Book of Silicon Photonics*, Chapter 9, pp 439-478, 2013 (CRC Press, Taylor & Francis Group).

10. Park S, Yamada K, Tsuchizawa T, Watanabe T, Shinojima H, Nishi H, Kou R, Itabashi S, Influence of carrier lifetime on performance of silicon p-i-n variable optical attenuators fabricated on submicrometer rib waveguides, *Opt Express*, 18(2010)11282-11291.
11. Morichetti F, Melloni A, Ferrari C, Martinelli M, Error-free continuously-tunable delay at 10 Gbit/s in a reconfigurable on-chip delayline, *Opt Express*, 16(2008)8395-8405.
12. Sun P, Reano R M, Sub-milliwatt thermo-optic switches using free-standing silicon-on-insulator strip waveguides, *Opt Express*, 18(2010)8406-8411.
13. Suzuki K, Tanizawa K, Matsukawa T, Cong G, Kim S.-H., Suda S, Ohno M, Chiba T, Tadokoro H, Ohno M, Chiba T, Tadokoro H, Yanagihara M, Igarashi Y, Masahara M, Namiki S, Kawashima H, Ultra-compact 8×8 strictly-non-blocking Si-wire PILOSS switch, *Opt Express*, 22(2014)3887-3894.
14. Dong P, Qian W, Liang H, Shafiha R, Feng D, Li G, Cunningham J E, Krishnamoorthy A V, Asghari M, Thermally tunable silicon racetrack resonators with ultralow tuning power, *Opt Express*, 18(2010)20298-20304.
15. Leuthold J, Koos C, Freude W, Nonlinear silicon photonics, *Nature Photonics*, 4(2010)535-544.
16. Navalakhe R K, Gupta Nandita Das, Das B K, Fabrication and Characterization of Straight and Compact S-bend Optical Waveguides on a Silicon-on-Insulator Platform, *App Opt*, 48(2009)G125-G130.
17. George J P, Dasgupta N, Das B K, Compact integrated optical directional coupler with large cross section silicon waveguides, *Proc SPIE*, 7719(2010)77191X-77191X.
18. Bhatt G R, Das B K, Demonstration of ITU channel interleaver in SOI with large cross section single mode waveguides, *Proc SPIE*, 8069(2011)806904-806904.
19. Krubhakar I S, Narendran R, Das B K, Design and fabrication of integrated optical 1x8 power splitter in SOI substrate using large cross-section single-mode waveguides, *Proc SPIE*, 8173(2011)81730C;doi:1117/12.898475
20. Bhatt G R, Sharma R, Karthik U, Das B K, Dispersion-Free SOI Interleaver for DWDM Applications, *J Lightwave Tech*, 30(2012)140-146.
21. Bhatt G R, Das B K, Improvement of polarization extinction in silicon waveguide devices, *Opt Commun*, 285(2012)2067-2070.
22. Chandran S, Das B K, Tapering and Size Reduction of Single-mode Silicon Waveguides by maskless RIE", OECC 2012 - OptoElectronics Communication Conference, Bexco, Busan Korea, July 02-06, 2012.
23. Sasikumar H, Venkitesh D, Das B K, Highly efficient DBR in silicon waveguides with eleventh order diffraction, SPIE Photonics West 2013, San Francisco, CA, USA, 2-7 February 2013 (Paper 8629-16)
24. Karthik U, Das B K, Polarization-independent and dispersion-free integrated optical MZI in SOI substrate for DWDM applications, SPIE Photonics West 2013, San Francisco, CA, USA, 2-7 February 2013 (Paper 8629-35).
25. Sakthivel P, Dasgupta N, Das B K, Simulation and experimental studies of diffusion doped p-i-n structures for silicon photonics, SPIE Photonics West 2013, San Francisco, CA, USA, 2-7 February 2013 (Paper 8629-33).
26. Joshi R, B K, Gupta N D, Design of 2D Photonic crystals for integrated optical slow light applications, IWPSD-2013, Noida, India, Dec 2013.
27. Chandran S, Kaushal S, Das B K, Monolithic integration of micron to submicron waveguides with 2D mode-size converters in SOI platform, (Invited Talk), SPIE Photonics West 2014, San Francisco, CA, USA, 1-6 Feb 2014.
28. Ravindran S, Das B K, Design and fabrication of 8-channel AWGs with 2- μ m-SOI for optical interconnects, SPIE Photonics West 2014, San Francisco, CA, USA, 1-6 February 2014.
29. Ravindran S, Das B K, Modeling and Phase Error Analysis of AWG in SOI using Gaussian Beam Approximation, 12th International Conference on Fibre Optics and Photonics, Kharagpur, India , 13-16 December 2014 (Paper-T3A.67).
30. Kaushal S, Das B K, Design of maximally flat delay lines using apodized CROW structure in SOI, 12th International Conference on Fibre Optics and Photonics, Kharagpur, India , 13-16 December 2014 (Paper- 4B.3).
31. Sidharth R, Das B K, Semi-analytical model of arrayed waveguide grating in SOI using Gaussian beam approximation, *Appl Opt*, 54(2015)2158-2163.
32. Chandran S, Das B K, Surface trimming of silicon photonics devices using controlled reactive ion etching chemistry, *Photonics and Nanostructures – Fundamentals and Applications*, 15(2015)32-40.

33. Chandran S, Sundaram S M, Das B K, Method and apparatus for modifying dimensions of a waveguide, Patent Filed – 3799/CHE/2015.
34. Celler G K, Cristoloveanu Sorin, Frontiers of silicon-on-insulator, *J Appl Phys*, 93(2003)4955-4978.
35. Hsu S.-H, Tseng S.-C, You H.-Z, Birefringence characterization on soi waveguide using optical low coherence interferometry, in 7th IEEE International Conference on Group IV Photonics, 2010.
36. Khilo A, Popović M A, Araghchini M, Kärtner F X, Efficient planar fiber-to-chip coupler based on two-stage Silicon Photonics Technology: Ten Years of Research at IIT Madras 955 adiabatic evolution, *Opt Express*, 18(2010)15790-15806.
37. Asghari M, Krishnamoorthy A V, Silicon photonics: Energy-efficient communication, *Nature Photonics*, 5(2011)268-270.
38. Bogaerts W, Heyn P De, Vaerenbergh T Van, Vos K De, Selvaraja S Kumar, Claes T, Dumon P, Bienstman P, Thourhout D Van, Baets R, Silicon microringresonators, *Laser & Phot Rev*, 6(2012)47-73.
39. Xu Dan-Xia, Densmore A, Waldron P, Lapointe J, Post E, Delâge A, Janz S, Cheben P, Jens P, Schmid H, Lamontagne B, High bandwidth SOI photonic wire ringresonators using MMI couplers, *Opt Express*, 15(2007)3149-3155.
40. Thomson D J, Hu Y, Reed G T, Fedeli Jean-Marc, Low Loss MMI Couplers for High Performance MZI Modulators, *IEEE Photonics Technology Letters*, 22(2010)1485-1487.
41. Pathak S, Vanslebrouck M, Dumon P, Thourhout D V, Bogaerts W, Optimized Silicon AWG With Flattened Spectral Response Using an MMI Aperture, *J Lightwave Tech*, 31(2013)87-93.
42. Soldano L B, Pennings E C M, Optical multi-mode interference devices based on self-imaging: principles and applications, *J Lightwave Tech*, 13(1995)615-627.

[Received: 30.7.2016]